UM-P-79/30

ON THE STRUCTURE OF THE INCOMMENSURATE SUPERLATTICES OF 2H - $TaSe_2$

R. L. Withers and L. A. Bursill

School of Physics
University of Melbourne
Parkville, 3051, Victoria
Australia

Abstract

Reinterpretation of the neutron diffraction study of 2H-$TaSe_2$ by Moncton, Axe and DiSalvo (1977) reveals an ambiguity in the sense of the displacements proposed for the commensurate superlattice structure. We attempt to resolve this ambiguity by electrostatic and short-range energy calculations of the phase dependence of the energy of the periodic structural distortion wave. There is a fine balance between Se-Se short range repulsion, Ta-Se electrostatic and short-range repulsion and the CDW-Ta ion interaction energy terms. The analysis reveals the phase dependence of the various terms and allows the different contributions to the stability of the distortion waves to be discussed more completely than previously. It is shown that the phase of the PSW/CDW wave is determined to π rad by minimumizing (harmonic) energy terms, which vary as the square of the PSD wave amplitude. This phase relationship is established above the normal/incommensurate onset temperature T_o. The π ambiguity is then resolved finally at the incommensurate/commensurate transition temperature T_c, by minimumizing the (anharmonic) energy terms which vary as the third power of the PSD wave amplitude.

Our analysis leads naturally to a new structural model for the incommensurate superlattice structure for $T_c \leq T \leq T_o$, involving contributions from both the preferred phase ϕ and the phase $\phi \pm \pi$ which simply corresponds to changing the sign of all displacements. The model is the logical consequence of a "softening-mode" phase transition and provides a very simple structural explanation for the observed incommensurate superlattice periodicity, 2.98 a at onset, and its temperature dependence.

1. Introduction

Despite widespread theoretical interest in the phase transitions and physical properties of the transition metal dichalcogenides (see e.g. Triste (Ed.) 1978 and recent reviews by Bruce, Cowley and Murray, 1978) it is disturbing that there appears to be only one attempt to determine the atomic displacements in the commensurate (or incommensurate) phases by use of standard X-ray or neutron diffraction techniques of structure analysis. This is the neutron diffraction study of the commensurate superlattice in 2H-$TaSe_2$ by Moncton, Axe and DiSalvo, 1977. The superlattice intensities indicated that the atomic displacements are predominantly longitudinal with the symmetry of the normal mode Σ_1. The atom labelling scheme and axial system is shown in Fig. 1. Moncton *et al* assumed that an eigenvector $\underline{e}_K$ transforming as a single representation would adequately describe the commensurate superlattice. Symmetry constraints reduced the number of independent atomic displacement parameters to six, representing the amplitudes and phases of the Ta motion in the $\hat{\underline{x}}$ direction $(\varepsilon_{1_x}, \phi_{1_x})$, Se motion in the $\hat{\underline{x}}$ $(\varepsilon_{3_x}, \phi_{3_x})$ and z directions $(\varepsilon_{3_z}, \phi_{3_z})$. Expressions for the superlattice structure factors were developed using atomic displacements given by

$$\underline{u}_{\ell K} = \sum_{\underline{q}} \tfrac{1}{2} \left(\underline{e}_K(\underline{q}) \exp(i\underline{q}.\underline{R}_\ell) + \underline{e}^*_K(\underline{q}) \exp(-i\underline{q}.\underline{R}_\ell) \right) \qquad (1)$$

for the K^{th} atom in the ℓ^{th} unit cell for a normal mode of wave vector $\underline{q}$ containing contributions from each of the three symmetrically equivalent wave vectors $\underline{q}_1$, $\underline{q}_2$ and $\underline{q}_3$. The eigenvector components

$$\underline{e}_{K\alpha} = \epsilon_{K\alpha} \exp(i\phi_{K\alpha}) \tag{2}$$

and the convention

$$\underline{e}^{*}_{K}(\underline{q}) = \underline{e}_{K}(-\underline{q}) \tag{3}$$

was adopted. The numerical values of $(\epsilon_{K\alpha}, \phi_{K\alpha})$ for $TaSe_2$ at 5K given in Table 1 of Moncton et al were found to be inconsistent with the displacements shown in their Fig. 9 and with their calculated structure factors (Moncton et al, Fig. 8). By fitting the observed structure factor data (op cit a calculator) two numerical errors (presumably misprints) were found in their Table 1. The corrected values are

$$\epsilon_{1_x} = -0.048, \quad \phi_{1_x} = -0.80;$$

$$\epsilon_{3_x} = 0.009, \quad \phi_{3_x} = 1.036;$$

$$\epsilon_{3_z} = -0.0172, \quad \phi_{3_z} = 0.28 \tag{4}$$

The remaining components are given by

$$\epsilon_{1_x} = \epsilon_{2_x}; \quad \phi_{1_x} = -\phi_{2_x}$$

$$\epsilon_{3_x} = \epsilon_{4_x} = \epsilon_{5_x} = \epsilon_{6_x}; \quad \phi_{3_x} = \phi_{4_x} = -\phi_{5_x} = -\phi_{6_x}$$

$$\epsilon_{3_z} = -\epsilon_{4_z} = -\epsilon_{5_z} = \epsilon_{6_z}; \quad \phi_{3_z} = -\phi_{5_z} = -\phi_{6_z} \tag{5}$$

all others being zero. Since it was not possible to accurately obtain absolute values for the weak superlattice reflections relative to the strong subcell reflections the above displacement magnitudes represent a lower limit and an approximate upper limit of 1.9 times these values was given.

It should be noted that the results of an analysis of Raman scattering data for 2H-$TaSe_2$ by Holy, Klein, McMillan and Meyer, 1976, showed that inversion symmetry is maintained in the superlattice phase. This imposes the condition

$$\underline{e}_K(\underline{q}) = -\underline{e}_K(-\underline{q}) \qquad (6)$$

Moncton et al claimed that the fit was insensitive to a change in the overall phase of the eigenvector

$$\underline{e}_K \rightarrow \underline{e}_K \exp(i\phi) \qquad (7)$$

and chose $\phi = -90^o$. However the transformation (7) is only strictly true for the ideal incommensurate superlattice, which is invariant under this transformation. We find that changing ϕ from -90^o to $+90^o$, for example, produces a change of 37% in the intensity of the (501) reflection for the commensurate superlattice, which is outside the error limits reported by Moncton et al. A comparison of other $|F|^2$ values for $\phi = -90^o$ is given in Table 1. It will be seen that in general the fit is insensitive to ϕ. More precise $(\varepsilon_{K\alpha}, \phi_{K\alpha})$ values might have been obtained if the condition (7) had been used in the least squares fit. (However the experimental accuracy and reproducibility of the measured superlattice

intensities may not have warranted this.) On the other hand it is clear from Table 1 that the absolute value of ϕ could have been obtained by fitting accurate values of the strong subcell reflections. We believe the corresponding X-ray diffraction experiment has been performed by Jellinek (private communication, 1979) whose conclusion was that $\phi = +90^{o}$, and not -90^{o}, which is equivalent to reversing the signs of all of the displacements $\underline{u}_{\ell k}$.

In this paper we first show analytically that Holy et al's inversion condition is equally consistent with $\phi = +90^{o}$ and thus Moncton et al's analysis leaves the sense of the atomic displacements undetermined. We then present an analysis of the change in cohesive energy of the commensurate superlattice structure relative to the normal state. This analysis makes explicit the phase dependence of the various terms. It is shown that ϕ must be + or -90^{o} in order to minimumize energy terms which vary as the square of the amplitude of the periodic structural distortion wave. It is the energy terms which vary as the third power of this amplitude which lift the ambiguity between $\phi = +$ and -90^{o}. Our analysis naturally suggests a new approach to the structure of the incommensurate superlattice and it is the development of such a model which is the major aim of this paper.

2. Ambiguity in structure due to inversion centre

It is clear from Fig. 1 that the inversion centre must lie midway between Ta atoms 1 and 2, in the centre of the empty octahedrally coordinated site between the trigonal prismatic layers. Thus the atom pairs 1 and 2, 3 and 6 and 4 and 5 are related by the inversion operation and

$$\underline{u}_{p\ell\alpha} = -\underline{u}_{q\bar{\ell}\alpha} \qquad (8)$$

where p = 1, 3, 4 and q = 2, 6, 5 are atom labels (see Fig. 1). We note from (5) that $\phi_{p\alpha} = -\phi_{q\alpha}$ and $\epsilon_{px} = \epsilon_{q\alpha}$. Thus using (1) and introducing the factor exp (iϕ) on both sides of (8) we find that ϕ must satisfy

$$\sum_{\underline{q}} \epsilon_{\underline{p}\alpha} \cos(\underline{q}.\underline{R}_{\ell} + \phi_{p\alpha} + \phi) = -\sum \epsilon_{\underline{p}\alpha} \cos(-\underline{q}.\underline{R}_{\ell} - \phi_{p\alpha} + \phi)$$

whence

$$\phi = +90^{o} \text{ or } -90^{o} \qquad (10)$$

Table 1 shows that $|F|^2$ values calculated using $\phi = \pm 90^{o}$ are equally consistent with the data, within experimental error. More accurate measurements, especially of the subcell reflections are required to distinguish between these two values of ϕ. Inspection of Moncton et al's Fig. 9 immediately confirms that reversal of sign of all displacements does generate a distinct crystal structure.

3. Electron density distribution

The natural parameter is the d-band conduction electron density

$$\rho(r) = \rho_{o}(r) \; [1 + \alpha(r)] \qquad (11)$$

where $\rho_{o}(r)$ is the normal d - electron density and $\alpha(r)$ may be expressed in terms of three sinusoidal CDW's having wave vectors $\underline{q}_i$ (i= 1,2,3) lying in the basal plane and in directions making angles of 120^{o} to each other. Thus

$$\alpha(\underline{r}) = \Sigma_i \rho_i \sin (\underline{q}_i . \underline{r} + \phi_i) \qquad (12)$$

where ρ_i and ϕ_i are the amplitudes and phases of the i^{th} component of the CDW triplet. It can be shown (see Appendix I) that the electron density distribution generated by the triplet $\underline{q}_i$ with arbitrary phases ϕ_i is identical with that produced by a triplet

of wave vectors $\underline{q}_i'$ having identical amplitudes to $\underline{q}_i$ but having three identical phases $\phi' = \phi_i'$ given by

$$\phi' = (\phi_1 + \phi_2 + \phi_3)/3 + 2/3\ (n+m)\pi \qquad (13)$$

where m,n are integers and the wave vectors $\underline{q}_i'$ are referred to an origin shifted by vector $\underline{r}'$ given by

$$\underline{r}' = \lambda/3\pi[\phi_3 - \phi_1 + 2n\pi]\hat{\underline{q}}_1 + \lambda/3\pi[\phi_3 - \phi_2 + 2\pi(n-m)]\hat{\underline{q}}_2 \quad (14)$$

where $\hat{\underline{q}}_i$ are unit vectors parallel to $\underline{q}_i$ and λ is the wavelength of the CDW's. In fact values of ϕ, $\phi + 120^\circ$ and $\phi + 240^\circ$, corresponding to $(n+m) = 0,1,2$ respectively, generate idential electron density distributions at three non-equivalent points A, B and C within the superlattice unit cell, corresponding to origin shifts $\underline{r}' = 0$, $\pm 2/3\lambda(\hat{\underline{q}}_1 + \hat{\underline{q}}_2)$ (Fig. 2). Other values of (m,n) generate electron density distributions indistinguishable from those at points A, B and C, since the origin shift simply amounts to a superlattice translation vector. For example m = 1, n = 2 gives $\underline{r}' = 2/3\ (2\hat{\underline{q}}_1 + \hat{\underline{q}}_2)$ as shown in Fig. 2 (a).

Fig. 2 shows an electron density contour plot (assuming ρ_i = 1 electron unit) for $\phi = +90^\circ$. Note the density maxima having 6-fold symmetry at points A and the two minima having trigonal symmetry at points B and C. Changing ϕ by 120° or 240° simply amounts to shifting the origin from point A to points C or B respectively. (Such shifts will become important later when we discuss models for the incommensurate superlattice structure). Figs. 3 (a) (b) show electron density profiles along $\underline{q}_1$ and $\underline{q}_1 - \underline{q}_3$ directions for $\phi = +90^\circ$.

We note that changing from $\phi = +90^\circ$ to $\phi = -90^\circ$ simply changes the sign of all of the peaks shown in Figs. 2 and 3(a)(b).

4. Atomic displacements for $\phi = \pm 90^{o}$

The displacements of Ta and Se atoms parallel to the basal plane were calculated using the parametres($\epsilon_{\kappa\alpha}$,$\phi_{\kappa\alpha}$) determined by Moncton et al. Thus

$$\underline{u}_{Ta}(\underline{r}) = 0.048\ \Sigma_i \hat{\underline{q}}_i \cos\ (\underline{q}_i.\underline{R}_\ell + \phi_{Ta}) \qquad (15)$$

where $\phi_{Ta} = \phi_{1x} + 180^{o} + \phi = 224.16^{o}$ for $\phi = +90^{o}$

and $\phi_{Ta} = \phi_{1x} + 180^{o} + \phi = 44.16^{o}$ for $\phi = -90^{o}$

The Ta atoms at the A,B and C sites are unmoved since the CDW electron distribution has zero gradient at these points. The Ta atom at $\underline{r} = (2\lambda/9)\ (\hat{\underline{q}}_1 - \hat{\underline{q}}_3)$ has displacement

$$\underline{u}\ (2/9\ \lambda[\hat{\underline{q}}_1 - \hat{\underline{q}}_3]) = (3/2)0.048\ [\hat{\underline{q}}_2\cos\phi_{Ta} + 1/\sqrt{3}(\hat{\underline{q}}_3 - \hat{\underline{q}}_1)\ \sin\ \phi_{Ta}] \qquad (16)$$

Since $\hat{\underline{q}}_2$ and $\underline{1}/\sqrt{3}\ (\hat{\underline{q}}_3 - \hat{\underline{q}}_1)$ are orthogonal unit vectors then this displacement has magnitude 0.072 Å and is directed at angle ϕ_{Ta} to $\hat{\underline{q}}_2$ (Fig. 4(a)). The displacement of the remaining 5 Ta atoms in the 3x3 superlattice unit cell are simply obtained by applying Σ_1 symmetry operations and these are shown in Fig. 4 (a). (Fig. 4 assumes $\phi = +90^{o}$, all displacements simply change sign for $\phi = -90^{o}$)

The Se displacements are given by

$$\underline{u}_{Se}(\underline{r}) = -\ 0.009\ \Sigma_i \hat{\underline{q}}_i \cos(\underline{q}_i.\underline{R}_\ell + \phi_{Se}) \pm 0.0172\ \Sigma_i \hat{\underline{z}} \cos(\underline{q}_i.\underline{R}_\ell + \phi_z)\ . \qquad (17)$$

where the $\pm$ signs refer to sheets of Se atoms labelled 3 and 4 respectively in Fig. 1. Now for $\phi = +90^{o}$ we find $\phi_{Se} = \phi_{3x} + 180^{o} + \phi = 329.36^{o}$

and $\phi_z = \phi_{3z} + 180^{o} + \phi = 286.04^{o}$

and there are three distinct types of displacements in the asymmetric unit, as shown in Fig. 1 (b) and (c) for the vertical and horizontal

components respectively. The latter show a remarkable degree of cooperative movement of the Se ions between layers, suggesting that short-range Se-Se interactions may be important in determining ϕ_{Se} and ϕ_z, and ultimately in establishing the phase of the CDW w.r.t. the lattice. Further evidence for strong short-range Se-Se forces is shown by the nature of the distortions of the octahedral interstices within the Se layers, labelled 4 and 5 in Fig. 1. Note especially the small centrosymmetric contraction (both horizontally and vertically) about A' in Fig. 4(c) and the much larger noncentrosymmetric displacements centred on B' and C'.

5. Cohesive Energy Calculations.

(a) Ta-Ta electrostatic interaction. The difference in electrostatic energy per unit cell between the normal (undistorted) structure and the 3 x 3 commensurate superlattice was calculated using

$$\Delta U^{C}_{Ta\text{-}Ta} = \tfrac{1}{2} \Sigma_{i,j} Q^2_{Ta} \left(1/R'_{ij} - 1/R_{ij} \right) \qquad (18)$$

where R_{ij} and R'_{ij} are the initial and final Ta-Ta interatomic spacings respectively and Q_{Ta} is the effective charge on the Ta atom, assumed to be the same for all 9 Ta atoms per cell. Since the difference $R'_{ij} - R_{ij}$ is very small the sum Eq.(18) converges rapidly and summing to 6th nearest neighbours yields

$$\Delta U^{C}_{Ta\text{-}Ta} = Q^2_{Ta} \left(1.373\, \epsilon^2_{Ta} + 0.0027\, \epsilon^3_{Ta} \sin 3\phi_{Ta} + \ldots \right). \qquad (19)$$

The short-range Ta-Ta interaction term is insignificant so that the phase dependence of the Ta-Ta interaction is carried by the cubic

(anharmonic) term which is minimumized for ϕ_{Ta}=90°, 210° or 330°.

(b) Ta-Se electrostatic and short-range interactions. The electrostatic contribution was calculated using an expression similar to Eq. (18). For the short-range terms an interaction potential $\lambda \exp\{-R/\sigma\}$ was chosen, where R is the interatomic separation and λ and σ are constants. Thus the change in short-range energy is

$$\Delta U^{SR}_{Ta\text{-}Se} = \Sigma_{i,j}\, k_{Ta\text{-}Se} \{ \exp((R_o - R'_{ij})/\sigma) - 1\} \qquad (20)$$

where R_o is the normal state bond length (2.597 Å), $R_o - R'_{ij}$ is the change in bond length and $k_{Ta\text{-}Se} = 0.385|Q_{Ta}Q_{Se}|$ is determined by the effective charges Q_{Ta} and Q_{Se} of the Ta and Se atoms. (This value of $k_{Ta\text{-}Se}$ was obtained by requiring

$$\frac{\partial}{\partial R}\{ -|Q_{Ta}Q_{Se}|/ R + k_{Ta\text{-}Se} \{\exp(R_o - R)/\sigma - 1\}\}_{R=R_o} = 0,$$

whence $k_{Ta\text{-}Se} = (\sigma/R_o^2)|Q_{Ta}Q_{Se}| = 0.0385|Q_{Ta}Q_{Se}|$, assuming $\sigma/R_o = 0.10$ (Kittel, 1976). The phase dependence is relatively insensitive to σ/R_o since the trigonometric arguments are not effected, and the coefficients of the various terms change only slightly.)

Thus the total change in cohesive energy, electrostatic plus short-range, and including terms to second nearest neighbours, is

$$\Delta U^{TOT}_{Ta\text{-}Se} = k_{Ta\text{-}Se}\{ 139.10\, \epsilon_z^2 + 90.99\, \epsilon_{Se}^2 + 121.41\, \epsilon_{Ta}^2$$

$$+(210.44 \sin(\phi_z - \phi_{Ta} + 200^o) + 12.57 \sin(\phi_z + \phi_{Ta} + 320^o))\epsilon_z\, \epsilon_{Ta}$$

$$+(3.14 \sin(\phi_{Se} - \phi_{Ta} + 180^o) - 136.23 \sin(\phi_{Se} - \phi_{Ta} + 320^o))\epsilon_{Se}\, \epsilon_{Ta}$$

$$+ 42.55 \sin(3\phi_z + 60^o)\,\epsilon_z^3 + 34.83 \sin(3\phi_{Se} + 60^o)\,\epsilon_{Se}^3$$

$$+ 92.75 \cos(3\phi_{Ta})\epsilon_{Ta}^3$$

$$+ (0.42 \sin(\phi_{Ta} + 2\phi_z + 10^o) - 161.46 \sin(\phi_{Ta} + 2\phi_z + 130^o))\epsilon_z^2\epsilon_{Ta}$$
$$- (137.03 \sin(\phi_{Se} + 2\phi_{Ta} + 220^o) + 58.79 \sin(\phi_{Se} + 2\phi_{Ta} + 200^o))\epsilon_{Se}\epsilon_{Ta}^2$$

$$- (54.39 \sin(\phi_{Ta} + 2\phi_{Se} + 220^o) + 67.50 \sin(\phi_{Ta} + 2\phi_{Se} + 10^o)$$

$$+ 1.97 \sin(\phi_{Ta} + 2\phi_{Se} + 250^o) - 3.22 \sin(\phi_{Ta} + 2\phi_{Se} + 100^o))\epsilon_{Se}^2\epsilon_{Ta}$$

$$- (51.24 \sin(\phi_z + \phi_{Se} + \phi_{Ta} + 130^o) + 229.85 \sin(\phi_z + \phi_{Se} + \phi_{Ta} + 250^o))$$

$$(\epsilon_z\,\epsilon_{Se}\,\epsilon_{Ta}) + \ldots \}. \qquad (21)$$

The quadratic (harmonic) terms are minimumized for $\phi_{Se} - \phi_{Ta} = 131^o$ and $\phi_z - \phi_{Ta} = 67^o$, which should be compared with Moncton et al's values $\phi_{Se} - \phi_{Ta} = 105.20^o$ and $\phi_z - \phi_{Ta} = 61.38^o$. The absolute values of ϕ_{Se}, ϕ_z and ϕ_{Ta} are not determined by minimumizing these harmonic terms since the phase differences $\phi_{Se} - \phi_{Ta}$ and $\phi_z - \phi_{Ta}$ are insensitive to an arbitrary phase shift ϕ.

(c) Se-Se interactions. The intralayer Se-Se electrostatic and short-range interactions, both within layers such as 4 or between layers such as 3 and 4 (see Fig. 1), have no quadratic phase dependent terms. (The corresponding cubic terms are discussed in section 5(e) below.) There is however a second-order term for the Se-Se

inter-layer short-range interaction, i.e. between the close-packed Se-Se layers 4 and 5. (The weak interlayer van der Waals interaction is assumed negligible.) Thus for the interlayer Se-Se interactions we obtain

$$\Delta U^{SR}_{Se\text{-}Se} = k_{Se\text{-}Se}\{\, 138.96\,\varepsilon_z^2 - 20.90\,\varepsilon_{Se}^2 + 80.24\,\varepsilon_z^2 \sin(2\phi_z + 100^o)$$

$$- 12.06 \sin(2\phi_{Se} + 220^o)\,\varepsilon_{Se}^2$$

$$+ 20.22 \sin(2\phi_{Se} + 220^o)\,\varepsilon_{Se}^2$$

$$- 127.18\varepsilon_{Se}\,\varepsilon_z \sin(\phi_{Se} + \phi_z + 160^o) + \ldots\} \quad (22)$$

It is interesting to note that the experimental values $\phi_z = 286^o$ and $\phi_{Se} = 329^o$ are surprisingly close to those values obtained by minimumizing $\sin(2\phi_z + 100^o)$ and $\{-12.06 \sin(2\phi_{Se} + 100^o) + 20.22 \sin(2\phi_{Se} + 220^o)\}$ separately, i.e. $\phi_z' = 265^o$ and $\phi_{Se}' = 313.5^o$. (Inclusion of the remaining term containing $\sin(\phi_{Se} + \phi_z + 160^o)$ in the minimumization would give even better agreement.) Note that values of ϕ_z and ϕ_{Se} obtained by minimumizing Eq.(22) are sensitive to an arbitrary overall phase shift ϕ, but are not sensitive to a shift of π, because of the $\sin 2\phi$ dependence of each term in Eq.(22). Thus it is the short-range Se-Se interlayer interactions which determine ϕ_{Se} and ϕ_z. ϕ_{Ta} is then determined by the intralayer Ta-Se interactions, which determine $\phi_{Se} - \phi_{Ta}$ and $\phi_z - \phi_{Ta}$.

(d) CDW - Ta interaction energy. We assume here that the CDW is localized in the Ta metal atom layers and we neglect any direct CDW-Se interaction energy. Some justification for this assumption

comes from XPS studies of 1T-TaS_2 (Hughes and Pollack, 1978) who observed splittings of 4f-Ta, but not 2d-S levels due to the CDW. Such splittings were not observed for 2H-TaS_2 due, presumeably, to the small amplitude of the PSD wave in 2H. Given these assumptions we find

$$\Delta U_{CDW} = - Q_{Ta}(\rho^{CDW} / \epsilon_{Ta}) \{ - 18 \epsilon_{Ta}^2 \cos(\Phi_{CDW} - \Phi_{Ta}) + (9/2) \epsilon_{Ta}^3 \sin(\Phi_{CDW} + 2\Phi_{Ta}) + \ldots \} \quad (23)$$

where the amplitude ρ^{CDW} of the electron distribution is linear in ϵ_{Ta} to a first approximation (Moncton et al) so that in fact the leading phase dependent term is second order in ϵ_{Ta}. Minimumization of this term requires $\Phi_{CDW} = \phi_{Ta}$, although we again find that the difference $\Phi_{CDW} - \phi_{Ta}$ is insensitive to an arbitrary overall phase shift of ϕ in both Φ_{CDW} and ϕ_{Ta}.

(e) Discussion of the interaction energy terms.

(i) Harmonic terms. We have shown in sections (a) to (d) above that the relative values of the CDW phase Φ_{CDW} and the PSD phases ϕ_{Ta}, ϕ_{Se} and ϕ_z are determined by the quadratic energy terms, apart from a possible phase shift of π. Thus the quadratic terms in $\Delta U^{SR}_{Se\text{-}Se}$ determine the phases of the Se motion ϕ_{Se} and ϕ_z, $\Delta U^{TOT}_{Ta\text{-}Se}$ fixes the differences $\phi_{Ta} - \phi_{Se}$ and $\phi_{Ta} - \phi_z$ and hence ϕ_{Ta} and finally the CDW phase $\Phi_{CDW} \approx \phi_{Ta}$ in order to maximumize $|\Delta U|$. Realization that the relative values of the phases are determined by harmonic interaction energy terms has escaped previous authors. Thus McMillan and others (McMillan 1977; Moncton et al, 1977) use the Landau theory argument that the quadratic terms vanish at $T = T_o$ leaving

$$\Delta U = -b\varepsilon^3 + c\varepsilon^4 + \ldots \qquad (24)$$

so that the distortion wave amplitude (ε) is determined by the ratio of the cubic and quartic terms. They then assert that the relative phases are determined by the leading cubic term. However, our discussion above clearly shows that the quadratic terms determine the relative phases. This is easily reconciled with Landau theory by realizing that the relative phases of the Ta and Se motions for the Σ_1 mode are already determined for $T > T_o$ (after all the harmonic approximation does account for much of lattice dynamics). Thus above T_o the Σ_1 mode includes displacements of both $\pm \underline{u}(\underline{r})$, corresponding to $\phi = \pm 90^o$ respectively. Landau theory only requires that the total harmonic energy goes to zero at T_o, not that each contribution individually goes to zero. Thus the phase relationships will remain essentially unchanged for $T < To$ and softening of the Σ_1 mode will lead naturally to domains containing equal volumes of $\pm\underline{u}(\underline{r})$ displacements of $T = T_o$. We assert that the role of the anharmonic terms is simply to determine which of the two possible sets of displacements $\pm \underline{u}(\underline{r})$ is preferred as the PSD wave amplitudes ($\varepsilon_{k\alpha}$) increase with decreasing temperature, and thus determine the absolute values of the phases in the fully commensurate superlattice for $T < T_c$. We return to a detailed structural mechanism for the normal/incommensurate/commensurate phase transitions in § 6 below.

(ii) Anharmonic terms. We now consider the phase dependence of the cubic (anharmonic) interaction energy terms in an attempt to deduce the absolute phase relationship between CDW, PSD and the lattice.

We saw above(§ 5(a)) that the Ta-Ta electrostatic interaction term $\Delta U^C_{Ta\text{-}Ta}$ was minimumized for $\phi_{Ta} = 90^o$, 210^o or 330^o (Eq.(19)).

We have not attempted to directly minimumize the complex cubic terms (Eq.(21)) for the Ta-Se interactions. However, substitution of the experimentally observed amplitudes and phases ($\epsilon_{K\ell}, \phi_{K\ell}$) allows the Ta-Se interaction energy term to be calculated for the two possible values of the phase ϕ, i.e. $\phi = \pm 90^{o}$ respectively. Thus a sin 3ϕ phase dependence was obtained showing that $\phi = + 90^{o}$ maximumizes whereas $\phi = - 90^{o}$ minimumizes these cubic terms, giving $\sim \pm$ 2256 $k_{Ta\text{-}Se}\ \epsilon_{Se}^{3}$ respectively*. A similar procedure was

---

* The result has been simplified for comparison with $\Delta U^{SR}_{Se\text{-}Se}$ by noting that $\epsilon_{Ta}/\epsilon_{Se} = 4.619$ and $\epsilon_{z}/\epsilon_{Se} = 1.911$

---

repeated for the Se-Se cubic terms, including both interlayer and intralayer terms. In this case cos 3ϕ phase dependence was obtained so that this contribution is ~ 0 for both $\phi = \pm 90^{o}$ (numerically $\pm$ 34.99 $k_{Se\text{-}Se}\ \epsilon_{Se}^{3}$ for $\phi = \pm 90^{o}$). Thus the dominant lattice-lattice cubic term is the Ta-Se interaction. This is minimumized for $\phi = - 90^{o}$, corresponding to the arbitrary choice adopted by Moncton et al but contradicting, we believe, the X-ray analysis of Jellinek et al.

Finally we note that the Ta-CDW interaction (Eq.(23)) has phase dependence which is the inverse of that for the Ta-Se lattice interaction. Thus, not surprisingly, whichever value of ϕ maximumizes** the Ta-Se cubic terms simultaneously minimumizes the

---

** Maximumize and minimumize refer to absolute values, not moduli.

---

the CDW-Ta interaction, giving $\phi_{CDW} = \phi_{Ta} = 210^{o}$ and $\phi = + 90^{o}$. Thus if we

accept the conventional viewpoint that it is the CDW-Ta interaction which drives the transition (and hence we require this term to be minimumized) then our analysis favours $\phi = +90^{o}$. On the other hand if lattice-lattice interactions drive the transition we expect $\phi = -90^{o}$. The above calculations alone do not allow this question to be resolved : they are too simplistic, the effective charges and hence k_{Ta-Se} cannot be accurately determined, covalent bonding and temperature dependence have not been included. However, our calculations do give a reasonably complete physical picture of the factors determining ϕ_{CDW}, ϕ_{Se}, ϕ_{z} and ϕ_{Ta}. Furthermore the fine balance which exists between the anharmonic CDW-lattice and Ta-Se lattic-lattic interactions, depending on $\phi = \pm 90^{o}$, leads us intuitively to a new structural model for the incommensurate superlattice structure, described in the next section.

§6 Structure of the incommensurate superlattice at T_o.

(a) Neutron data and discommensuration models.

Realistic structural models for the incommensurate superlattice structure in 2H-$TaSe_2$ must explain the following observations of Moncton et al. The wavevector below the onset temperature T_o is not exactly commensurate, with $\underline{q}_c = (1/300)$, but is $\underline{q}_\delta = (1 - \delta)\underline{q}_c$, with $\delta \sim 0.025$ and temperature dependence as shown in Fig. 5(a). δ drops suddenly to 0 at $T_c = 90\,K$ suggesting a first-order incommensurate/commensurate transition. In the incommensurate state the primary lattice distortion wave vector $\underline{q}_\delta$ is accompanied by a weaker secondary distortion wave $\underline{q}_{2\delta} = (1+2\delta)\,\underline{q}_c$. The T_o transition appears continuous, i.e. second-order (see Fig. 5(a)).

The strength of the second order component increases with decreasing temperature as shown in Fig. 5(b)

Moncton et al and McMillan (1976) argued that a single plane wave with $q_\delta \lesssim q_c$ will have regions $\sim\lambda c/2$ over which the lock-in potential is alternatively attractive and repulsive and thus the existence of higher-order Fourier components in the distortion wave is expected on theoretical grounds. A theoretical analysis by Moncton et al constrained the distortion wave to have equal amplitude and phase components, whereas McMillan argued that a pure phase distortion would give a lower free energy. However, neither analysis gave good agreement with the observed temperature variation (see Fig. 5(a)). Thus Moncton et al predicted a sharp drop in δ from 0.020 rather than from 0.005 as observed, suggesting the commensurate state is far too strongly favoured by their model. McMillan's curve shows a continuous variation of δ for $T_c \leq T \leq T_o$, with opposite slope to the experimental curve, and shows no first-order behaviour for the T_c transition. Bruce, Cowley and Murray (1978) showed that coupling of a uniform macroscopic elastic strain to McMillan's pure phase discommensuration model does introduce a strong first order transition, but no calculated $\delta(T/T_c)$ curve was given. Bak and Timonen (1978) have further extended the theory to allow for an inhomogeneous soliton like strain with the adrupt $2\pi/3$ phase changes of the discommensurations. This restored the second-order nature of the T_c transition but again no attempt was made to predict the observed $\delta(T/T_c)$ variation.

It is not clear from McMillan's analysis why he chose a discommensuration model having $2\pi/3$ phase shifts, since he did not explicitly consider other possible values of $\Delta\phi$. Clearly such a model has a strong analogy to the antiphase domains or stacking

faults which occur in close-packed structures. For the CDW electron distribution in Fig. 2 there are three possible choices for the origin, separated by phase shifts of $\pm 2\pi/3$, and this suggests a possible domain structure. However no exhaustive search for other plausible structural models was undertaken. Fig. 6 shows a plot of the variation in electron charge density along $\underline{r} = x\lambda(\hat{\underline{q}}_1 - \hat{\underline{q}}_2)$, i.e. normal to McMillan's $2\pi/3$ discommensuration. Such soliton like behaviour for $\rho(\underline{r})$ seems to us most unlikely. What conceiveable distortion of the lattice, presumably involving very strong covalent bonds, could possibly sustain such a singularity in (conduction) electron density? We therefore searched for alternative discommensuration models which might minimumize $\underline{\nabla}\rho(\underline{r})$ across the domain boundaries. In fact such a model was immediately suggested by the $\pm\pi$ ambiguity discussed above and the well-known "softening-mode" nature of the phase transitions. Thus we were lead intuitively to consider discommensuration triplets which give a smooth variation in electron charge density across domain boundaries. Furthermore such a model immediately predicts a structural interpretation of the temperature variation of δ and to the mechanism of the T_o and T_c phase transitions.

(b) Systematic derivation of lowest energy discommensuration structures. The basis for this derivation is given in Figs. 2 and 3 which show the electron density distribution for $\phi_{CDW} = 210^o$ and the corresponding profiles along $\underline{r} = x\lambda\hat{\underline{q}}_1$ and $\underline{r}=x\lambda(\underline{q}_1 - \underline{q}_3)/\sqrt{3}$. We recall that $\phi_{CDW} = 210^o$ or 330^o simply correspond to origin shifts from points labelled A to those labelled B and C respectively. Domain boundaries delineating such phase shifts are simply McMillan's $2\pi/3$ discommensurations. Inclusion of the "soft-mode" equivalents

$\phi_{CDW} \pm \pi$ then leads to a total of six possible choices for the CDW origin in a domain structure, all of which retain Σ_1 mode symmetry and lead to centrosymmetric commensurate superlattices as required by the neutron and Raman scattering analyses.

(i) Domain walls perpendicular to $\hat{q}$. The domain walls may pass through A, B or C type sites and we first consider the 5 distinct A-type walls having phase shifts and labels as indicated in Table 2. Two dimensional electron density contours are given in Figs. 7 to 11. For each wall type we considered five important profiles, labelled 1 and 2 for $\underline{r} = x\lambda\hat{q}_1$ and a, b, and c for $\underline{r} = x\lambda(\hat{q}_1 - \hat{q}_3)/\sqrt{3}$, and these are also shown in Figs. 7 to 11. It is immediately apparent that the domain wall type A3 shows by far the best matching of $\Delta\rho$ across the domain wall. Furthermore profile A3-2 immediately suggests that contraction of the profiles by 0.0474 λ_{comm} on each side of the domain boundary would allow continuous matching of all five profiles with $\rho = 0$ at the domain wall. All other four models (A1, A2, A4, A5) predict cusp-like gradient changes for one or more of its profiles and in most cases these would give positive or negative peaks in ρ at the domain walls. None of these other models lead naturally to contraction or expansion of the CDW and hence do not lead to an explanation of the incommensurate superlattice periodicity. Fig. 12a,b shows a plot of profiles A3-1/2 with and without a linear contraction of the CDW according to

$$\lambda_{incom} = (1 - 0.0474)\ \lambda_c \qquad (25)$$

Note that the electron density smoothly goes to zero in the vicinity of the wall for A3-1 and gives zero gradient change across the domain wall for A3-2. Annihilation of ρ at the domain walls simply corresponds to insertion of a slab of normal (high-temperature) structure. This type of discommensuration model immediately predicts two of the essential features of an incommensurate CDW structure. Firstly, there is a uniform change in the CDW wavelength, in this case a contraction, given by

$$\delta = 0.0474 \times 2/p \qquad (26)$$

where P is the domain wall spacing, measured in units of λ. Secondly, there is a localized distortion of the CDW, in the immediate vicinity of the discommensuration, but this amounts only to retention of elements of the structure which existed above T_o. The CDW profiles possess the black and white symmetry operation m' (i.e. mirror combined with change in sign of the electron density, see Megaw (1973) or Bradley and Cracknell, (1972)) . Note that the models A1 and A4, which correspond to McMillan's discommensurations ($\Delta\Phi_{CDW} = \mp 120^o$ respectively) each contain 3 cusp-like functions in the profiles which would be most unstable w.r.t. A3. It should be noted that the diffraction evidence for 2H-$TaSe_2$ requires $\lambda_{incom} < \lambda_c$, i.e. we require expansion rather than contraction of the wavelength. This difficulty is overcome by consideration of B and C type discommensurations.

A study of profiles for B-type discommensurations did not yield any new possibilities for low energy boundaries requiring changes in CDW wavelength. For example Fig. 13 shows profiles and contour plot for the B1 type discommensuration (McMillan type,

$\Delta\Phi_{CDW} = -120^{o}$). Profiles B1 - a and b both show high energy cusps, whereas curves B1-1, 2 and c will be smoothest for CDW wavelength = λc and therefore will not lead to incommensurateness.

Finally we consider type C boundaries. These give profiles closely resembling those for type A, with the exception that CDW stretching, rather than contraction is required. The lowest energy boundary in this case is C4 ($\Delta\Phi_{CDW} = +60^{o}$, Fig. 14). Thus profiles C4-2 becomes virtually continuous for a uniform expansion of the CDW corresponding to

$$\delta = - 0.0474 \times 2/P \qquad (27)$$

Fig. 14 a, b, shows the result of smoothing profiles C4 - 1 and C 4 - 2 after uniform increase in CDW wavelength.

It is interesting to note that annihilation of the CDW electron density required for continuity of profiles C4 - 1 and C4 - 3, 4, 5 may be regarded as the result of attraction between equal and opposite charge densities at the domain wall or discommensuration. Thus in this case the incommensurate stretching of the CDW for profile C4 - 2 would seem to positively aid the annihilation, suggesting the origin of attractive energy terms which stabilize the incommensurate state for $T_c \leq T \leq T_o$.

(iii Domain boundary triplets normal to $\hat{q}_i$ In both 2H-$TaSe_2$ and 2H-$NbTe_2$ the value of δ at the onset temperature T_o is $\Delta = -0.025$. This immediately suggests by comparison with Eq.s (26) and (27) that we construct a two-dimensional type C4 domain boundary structure with domain boundary spacing, along $\hat{q}_i$, given by P = 4, yielding a predicted $\delta = -0.024$, in excellent agreement with the experimental value.

Taking $\phi_{CDW} = 210^{o}$ at the origin on a type C site we find that the distance to a domain boundary is given by

$$\underline{R}_i = p\lambda\hat{\underline{q}}_i \qquad (28)$$

where p may take the values

$$p = n + 1/3 \quad \text{or} \quad -n \text{ (n positive integers)} \qquad (31)$$

along the $\pm\ \hat{\underline{q}}_i$ directions respectively. In fact this asymmetric choice of origin (which in turn was dictated by the cohesive energy calculations above) leads to further multiplicity of 2 into the number of domain boundary phase relationships. Thus if the domain wall distance from the origin is given by $p = n + 1/3$ then the phase shift $\Delta\phi_{CDW} = +60^{o}$ as required by the profile analysis above (see Fig. 14). On the other hand if $p = -n$ then we generate <u>identical</u> domain walls but $\Delta\phi_{CDW} = -60^{o}$. This will be made clear by reference to Figs. 16 a, b which show the phase relationships for the trigonal domain structures obtained for $p = -2$ and $+2\ 1/3$ respectively. Note that the domain wall spacing (along $\hat{\underline{q}}_i$) is given by $P = 3p$ in each case. These two-dimensional domain structures are described by the black and white point group 3m'. Thus the observed value of δ at the onset temperature T_o, for both 2H-$TaSe_2$ and 2H-$NbSe_2$, immediately leads to the CDW model shown in Fig. 16(a). Note that ϕ_{CDW} is alternately 210^{o} and 150^{o} in adjacent trigonally arranged domains.

Attempts to draw alternative arrangements of domain walls and junctions, having the same phase relationship, were unsuccessful, since 3m' is the only two - dimensional black and white point group having trigonal symmetry, as required by the neutron amd Raman results.

It is important to realize that although the CDW is distorted (by an overall stretching as well as insertion of some normal structure near the domain walls) so that the mean wavelength is incommensurate, i.e.

$$\lambda_{incom} = (1 - \delta)\ \lambda_c \qquad (29)$$

in fact the crystallographic unit cell for the domain structure is commensurate, with

$$a_{-1} = 6a_{com} = 18\ a_{-N}\ (=61.9\ \text{Å}) \qquad (30)$$

where $a_{-N} = 3.44$ Å is the cell parameter for $T > T_o$. (We return to discuss the PSD wave for the ions and the consequences of the model for the diffraction intensities below.)

It is now necessary to consider the CDW phase relationship between adjacent trigonal prismatic layers of the structure. There are two possible positions for the location of the inversion centre required by the Raman results; i.e. at the centroid of each domain or at the domain wall junctions. Attempts to place an inversion centre at the centroid position generates a discontinuous arrangement of domain walls with those at layer I rotated by 30^o with respect to those on layer II and implies mixing of $p = -n$ and $p = n + 1/3$ structures on adjacent levels. This possibility is therefore self-contradictory and may be ruled out.

Location of the inversion operation at the wall junction leads to continuous domain walls parallel to the c axis, with the layers of Fig. 16 (a) exactly superimposed. (In fact ϕ_{CDW} changes by $\pm\ \pi$ in adjacent layers due to the translation vector of $\frac{1}{2}c$).

The black.and white space group would appear to be $P\bar{3}'1m'$ (Bradley and Cracknell, (1972)). We note that the inversion centre at the domain centroid must be recovered on lock-in to the commensurate ($x3a_{-N}$) superlattice. Its absence in the incommensurate state leads to minimumization of $\Delta U^{SR}_{Se\text{-}Se}$ (Eq. (22)) allowing perfect matching of the Se displacements in adjacent layers. Thus one would expect that the incommensurate state will be stabilized by high pressure in agreement with the observations of Chu, Testardi, DiSalvo and Moncton (1976), who found that T_o increases slightly whereas T_c decreases rapidly with increasing pressure.

The presence of the domain walls and junctions, where $\rho_{CDW} = 0$ is remarkably consistent with the interpretation of XPS measurements of Hughes and Pollak (1976) and the view of McMillan (1976), based on specific heat and energy gap measurements, that the coherence length in the incommensurate state is very small. The maximum domain area, at onset, for our model is $10.83\ a^2$, which compares favourably with McMillan's estimate of linear coherence length of $\sim 3a$!

§ 7 Temperature Variation of Incommensurate Superlattice Structure

(a) Domain structure

We have seen in §6 above that the domain wall separation P is directly related to δ so that δ could conceivably decrease to zero by increasing P from 4 to ∞ in integral steps. However, this does not increase the fraction of anharmonically favoured structure (say $\phi_{CDW} = 210^o$) at the expense of the alternative structure ($\phi_{CDW} = 150^o$) so that the $\phi = \pm\pi/2$ ambiguity would not

be resolved, even for infinite P. Furthermore such a model does not lead naturally to the introduction of a second harmonic into the CDW.

Fig. 17 (a) to (g) show an alternative approach whereby areas of the favoured structure (black) increase in area relative to areas of anharmonically unfavoured structure (white) in stages. The corresponding values of p , ϕ_{CDW} and relative areas of the different domains are given in Table 3. Note that in order to allow p to change in steps of 1/3 we require ϕ_{CDW} to advance by 120^{o} in successive stages, simultaneously in both black and white domains, so that $\phi_{CDW}^{black} - \phi_{CDW}^{white}$ remains constant at 60^{o}. The variation of ϕ_{CDW} with temperature in the two domains is shown schematically in Fig. 18. Of course there are a number of possible excitations of the incommensurate structures which may vary as the temperature decreases. The structure will not be static. Fig. 17 represents the average structure at various stages of decreasing temperature. We will not pursue such excitations in this paper.

(b) Variation of δ with domain size. Whereas the value of δ at the onset temperature T_o was predicted precisely (= 0.023) (see §6 (b) ii above) it is not possible to immediately assign values of δ to the intermediate stages shown in Fig. 17 (a) to (g). We therefore refer back to the neutron data. The abrupt decrease in δ at $T = T_c$ suggested that we assign $\delta = 0.005$ to the structure shown in Fig. 17 (f), i.e. the penultimate stage. The increase in amplitude of the second harmonic peak with decreasing temperature (Fig. 5 b) must also be explained by our structural model. We therefore introduced the second harmonic into the CDW as follows,

so as to make explicit its structural implications in an attempt to find a relationship between δ and p. Thus the electron density becomes

$$\rho(\underline{r}) = \rho_1 \Sigma_i \sin(\underline{q}_i \cdot \underline{r} + \Phi^1_{CDW}) + \rho_2 \Sigma_i \sin(2\underline{q}_i \cdot \underline{r} + \Phi^2_{CDW}) \qquad (31)$$

and along the direction $\underline{r} = - x\lambda_c \hat{\underline{q}}_1$

$$\rho(x) = \rho_1\{\sin(\Phi^1_{CDW} - 2\pi x(1 - \delta)) + 2 \sin(\Phi^1_{CDW} + \pi x(1 - \delta))\}$$

$$+ \rho_2\{\sin(\Phi^2_{CDW} - 4\pi x(1 - \delta)) + 2 \sin(\Phi^2_{CDW} + 2\pi x(1 - \delta)) \qquad (32)$$

where (ρ_1, Φ^1_{CDW}) and (ρ_2, Φ^2_{CDW}) are the amplitudes and phases of the first and second harmonics respectively. In order to assign values of Φ^2_{CDW} we plotted $\rho(x)$ using Eq.(32) for various values of ρ_2/ρ_1 and δ taken from Fig.5(a),(b). Thus for $T/T_o = 0.90$ the appropriate values are $\rho_2/\rho_1 = 0.27$ and $\delta = 0.010$. We assume $\Phi^1_{CDW} = 210^o$ as discussed in section 6-(b)ii above. Figs. 19a,b,c,d show plots of $\rho(x)$ for $\Phi^2_{CDW} = 30^o$, 150^o, 210^o, 330^o respectively. We find that only two values of Φ^2_{CDW} retain the hexagonal symmetry of the A site and retain equal charge density and trigonal symmetry at the B and C sites, i.e. $\Phi^2_{CDW} = 150^o$ and 330^o. (The general condition for these properties of the CDW to be retained is $2(\Phi^1_{CDW} - \Phi^2_{CDW}) = 120^o, 240^o, \ldots$) Figs 20a,b,c show the nature of the distortions in the CDW profile produced by the addition of a second harmonic. Thus Fig.20a shows the profile for $\rho_2 = 0$, $\rho_1 = 1.27$ and $\Phi^1_{CDW} = 210^o$ (i.e. no second harmonic) whereas Figs 20b,c show plots for $\rho_2/\rho_1 = 0.27$, $\Phi^1_{CDW} = 210^o$ and $\Phi^2_{CDW} = 150^o$ and 330^o respectively. In each case the peaks occur at identical values of x but the peak widths are broadened and narrowed for $\Phi^2_{CDW} = 150^o$ and 330^o respectively. In order to construct discommensurations having zero $\nabla\rho$ change at the domin walls we proceed as before by joining profiles for domains having phase differences of 60^o

(see §6 (b) above). Figs. 21 a to g show profiles corresponding to directions joining the domain centroids in Fig. 17 a to g. We find that the choice of phase $\Phi^2_{CDW} - \Phi^1_{CDW} = 120^o$ (i.e. peak narrowing see Fig. 20 c) causes δ to decrease to zero as the relative magnitude of the second harmonic increases. A geometric analysis of the profiles yields the result

$$\delta = 0.0231 - 0.0688\ (\rho_2/\rho_1) - 0.0048\ (\rho_2/\rho_1)^2 \qquad (33)$$

Thus $\delta = 0.005$ yields a calculated value of $\rho_2/\rho_1 = 0.26$ in good agreement with the measured value of 0.30*

---

*δ, being a geometrical parameter is known with far greater accuracy than ρ_2/ρ_1 which depends on the relative magnitudes of the intensities of the first and second order satellite reflections, see Moncton et al)

The values deduced for δ at each stage of the transformation from the incommensurate superlattice at T_o to the commensurate superlattice are indicated in Fig. 21 a to g.

(c) Effect of addition of second harmonic on Ta and Se displacements

A sharpening of the electron density peaks also occurs along the direction $\underline{r} = x\lambda_c\ (\hat{\underline{q}}_2 - \hat{\underline{q}}_3)$ (Fig. 25) The corresponding flattening of the valleys in between the peaks will tend to increase the magnitude of the Ta displacements since $\underline{\nabla}\rho$ is decreased. For example at $\underline{r} = \underline{a}$ and for $\delta\underline{\nu}$ o

$$\nabla\rho(\underline{r}=\underline{a}) = 3/2\rho_1(1 - 2\rho_2/\rho_1)\ [\hat{\underline{q}}_2 \cos 210^o + (\hat{\underline{q}}_3 - \hat{\underline{q}}_1)/\sqrt{3} \sin 210^o]$$

which is simply $(1 - 2\rho_2/\rho_1)$ times the value of $\underline{\nabla}\rho$ if there were no second harmonic. If $\Delta\underline{x}$ were directly proportional to $\underline{\nabla}\rho$ then we might expect t Ta displacements to be simply decreased by the

factor $(1 - 2\rho_2/\rho_1)$. However ϕ_{Ta} is also changed by the addition of the second harmonic (shown schematically in Fig. 23). Thus elastic energy released due to the decrease in the magnitude of the displacement will be offset by the increase in elastic energy required to rotate the direction of displacement (bond-bending energy). Clearly there will be restoring forces opposing this rotation due especially to Se-Se interactions and then Ta-Se interactions. There will also be displacements of Ta and Se atoms due to the presence of the incommensurate superlattice spacing. Initially at onset there will be inversion centres located at the domain wall junctions (centre of Fig. 18 a) and we expect larger atomic displacements for the atoms associated with the domain walls and junctions. However, since these involve sites where the electron density in the CDW has virtually anihilated to zero the Ta-CDW interaction will be small and such displacements will be relatively small. As the unfavourable domains shrink (Fig. 17 b - g) the inversion centre is retained in the same site but now we have black-on-black superposition from one layer to the next and the structure now gradually approaches the commensurate structure. The largest atomic displacements still remain at the triangular domain walls and vertices but these decrease as δ decreases. The driving force for the transformation is clearly the increasing magnitude of the anharmonic Ta-Se energy terms favouring black-on-black regions. This has to overcome the stability of the domain walls and the more favourable CDW-CDW interlayer interactions existing for black-on-white arrangement of alternate layers. Thus as ρ_2/ρ_1 increases, i.e. δ decreases, it costs more and more energy to convert unit area of black-on-white into black-on black. Thus the

$\delta(T/T_o)$ curve should have concave curvature in agreement with experiment. (We note that the analyses of McMillan and Nakanishi and Shika predicted convex curvature.)

In order to predict $\delta(T/T_o)$ according to our model we first require to deduce the Ta and Se atomic coordinates for the large cells shown in Fig. 17. This is a nontrivial problem and in any case we believe it is first necessary to seek further diffraction evidence using both X-ray and neutrons, and possibly using high-resolution electron microscopy, before embarking on further calculations of the atomic positions and energetics of this phase transition.

§8. Conclusion

Our attempts to resolve the ambiguity in sign of the atomic displacements in the commensurate superlattice structure have lead to a physically reasonable picture for the incommensurate superlattice structure and a structural explanation for the variation of δ with temperature. In fact introduction of our large superlattice unit cell, containing domains and domain walls shows that the intermediate structure for $T_c \leq T \leq T_o$ is in fact not strictly incommensurate. The term is a misnomer in fact. However, locally the CDW wavelength is stretched relative to that existing below T_c so that to a first approximation the superlattice peaks appear to be non-integral multiples of the fundamental $TaSe_2$ structure ($a \approx 3.44$ Å). Fig. 24 shows a schematic representation of the diffraction intensities which we expect for the larger commensurate superlattices shown in Fig. 17.

Clearly is is now necessary to reexamine these superlattice structures with diffraction techniques, probably with significantly better resolution than used so far. Further theoretical treatments

should be directed towards the remaining polytypic structures showing similar, apparently incommensurate behaviour.

ACKNOWLEDGEMENTS.

This work was supported financially be the Australian Research Grants Committee and the University of Melbourne. R. L. Withers is grateful for a Commonwealth Post-Graduate Research Award. We wish to thank Dr. A. E. C. Spargo for his interest and encouragement in this work.

REFERENCES

Bradley, C. J. and Cracknell, A. P. "The Mathematical Theory of Symmetry in Solids." Clarendon Press, Oxford (1972) pp569.

Bruce, A. D., Cowley, R.A. and Murray, A.F. (1978), J.Physics C: Solid State Physics 11, pp3591-3608.

Chu, C. W., Testardi, L.R., DiSalvo, F.J. and Moncton, D.E. (1976) Phys. Rev. B14, 464-467

Holy, J. A., Klein, M. V., McMillan, W.L. and Meyer, S.F. (1976) Phys. Rev. Letters 37, 1145-1148.

Hughes, H. P. and Pollak, R. A, (1976), Phil Mag 34 1028-1046.

Kittel, C. Solid State Physics 5th Edition, Wiley, N.Y., (1976) pp.89.

McMillan, W. L., (1977), Phys. Rev. B16 643-650

Megaw, H.D. "Crystal Structures - A Working Approach", Saunders, London (1973) pp 182

Moncton, D.E., Axe, J.D. and DiSalvo, F.J. (1977) Phys. Rev. B16 801-819

Riste, T. (Ed.) "Electron -Phonon Interactions and Phase Transitions", Nato Adv. Study Inst. Series B: Physics, Plenum Press N.Y.

Wakabayashi, N., Smith, H.G., and Nicklow, R.M. (1975) Phys. Rev B12, 659-663.

FIGURE CAPTIONS.

Fig. 1 — Crystal structure, atom labelling scheme and axial system for 2H polytype.

Fig. 2 — Positions of A, B, and C sites relative to Ta net. Electron density plot for one Ta layer for $\Phi_{CDW} = 90^{o}$. Note the six-fold symmetry at A, which has a maximum in electron density and the two minima at B and C, which each have trigonal symmetry. Origin shifts of $\underline{r}' = 0$, $\pm$ 2/3 $\lambda(\hat{\underline{q}}_1 + \hat{\underline{q}}_2)$ correspond to phase shifts of 0^{o}, $\pm$ 120^{o} in ϕ_{CDW}, thus interchanging origin between A B and C sites.

Fig. 3a, b — Electron density profiles along $\hat{\underline{q}}_1$ and $\hat{\underline{q}}_1 - \hat{\underline{q}}_3$, cf. directions labelled in Fig. 2b. Electron density unit is ρ_o.

Fig. 4a — Unit cell of commensurate superlattice structure showing relative magnitudes and directions of Ta displacements for $\phi = +90^{o}$ and data from Moncton et al

Fig. 4b — Se atom displacements projected along $[10\bar{1}0]$ showing cooperative movement of Se on adjacent levels. Atoms labelled as in Fig. 1.

Fig. 4c — Se atom displacements for two levels corresponding to top of one sandwitch and bottom of next. Ideally these would be h.c.p. In fact there is a very small contraction of octahedra centred on A' but much larger asymmetric displacements centred on B' and C'

Fig. 5a, b, — Temperature dependence of δ and ratio of amplitudes of second / first harmonic contributions to the electron density (data from Moncton et al, Fig. 4). Calculated curves for Moncton et al's one-dimensional and McMillan's three-dimension discommensuration models are indicated.

Fig. 6 — Electron density profile along $\underline{r} = x\lambda(\underline{q}_1 - \underline{q}_3)$ for McMillan's $2\pi/3$ discommensuration model. Note singularity at domain wall.

Figs.7 to 11 — Two-dimensional electron density contours for discommensuration models having domain walls passing through A type sites ($\Phi_{CDW} = 210^{o}$). Electron density profiles along lines labelled 1, 2 and a, b, c in the directions $\underline{r} = x\lambda\hat{\underline{q}}_1$ and $x\lambda(\hat{\underline{q}}_1 - \hat{\underline{q}}_3)/\sqrt{3}$ respectively. Note the nature of the resultant electron profiles at the domain walls (dotted). Profile labelled A3-2 immediately suggests the origin of an incommensurate distortion of the CDW. Profiles A3-1 and A3-a,b,c all show smooth annihilation (zero) of the CDW

at the domain walls. This should be compared to cusp-like variation for many of the other profiles.

Fig. 12a, b — Plots of profiles A3-1 and A3-2 with and without a linear contraction in the CDW wavelength (see Eq. (25)), showing annihilation in A3-1 and joining of $\Phi_{CDW} = 210^{o}$ and 150^{o} profiles in A3-2 with $\underline{\nabla}\rho = 0$ at domain wall.

Fig. 13 — Two dimensional contours and corresponding electron density profiles for a discommensuration passing through type B site. These do not lead to incommensurate distortion of CDW and contain cusps in electron density at domain walls.

Fig. 14. — Contour plots and electron density profiles for C4 type discommensuration ($\Delta\Phi_{CDW} = +60^{o}$). Profile C4 - 2 indicates origin of extension of CDW wavelength given by Eq. (27).

Fig. 15a, b, — Plots of profiles C2-1 and C2-2 with and without linear expansion of CDW wavelength corresponding to $\delta = -0.0462 \times 2/P$, showing smooth annihilation of C2-1 and joining of $\Phi_{CDW} = 210^{o}$ and 330^{o} at domain wall with $\underline{\nabla}\rho = 0$.

Fig. 16a, b. — Domain structure at onset temperature T_o for $p = -2$ and 2 1/3 respectively. Note $\Delta\Phi_{CDW} = 60^{o}$ in each case and the black and white point group symmetry 3m'. Notice superlattice cell dimension

$$a_I = 6a_{com} = 18a_N = 61.9\ \text{Å}$$

Fig. 17a, g. Variation of domain structure for decreasing temperature. The displacements corresponding to the black domains are favoured by the anharmonic (cubic) Ta-Se interaction energy terms. (Corresponding values of p, Φ_{CDW} and the relative areas are given in Table 3.) Note that Φ_{CDW} advances by 120^o in each domain at each stage of the transformation.

Fig. 18 Variation of Φ_{CDW} with temperature.

Fig. 19a, b, c, d. Plots of electron density $\rho(-x\lambda_c\hat{q}_1)$ for CDW containing both first and second harmonics with $\Phi^1_{CDW} = 210^o$, $\Phi^2_{CDW} = 30^o$, 150^o, 210^o and 330^o respectively. Only $\Phi^2_{CDW} = 330^o$ gives correct symmetry for A B and C sites. Note narrowing of maxima and broadening of smaller peaks for $\Phi^2_{CDW} = 330^o$.

Fig. 20a,b,c. Distortion of CDW due to addition of second harmonic (a) shows electron density profile for $\rho_2 = 0$, $\rho_1 = 1.27$ and $\Phi^1_{CDW} = 210^o$ (b) shows cases for $\rho_2/\rho_1 = 0.27$, $\Phi^1_{CDW} = 210^o$ $\Phi^2_{CDW} = 150^o$ and 330^o respectively. Only $\Phi^2_{CDW} = 330^o$ gives correct sign for δ.

Fig. 21a to g Electron density profiles along lines joining domain centroids of Fig. 17 a to g respectively. δ decreases to zero according to Eq. (33), as indicated.

Fig. 22 Sharpending of maxima and broadening of valleys for electron density profile along $\underline{r} = x\lambda_c$ $(\hat{\underline{q}}_2 - \hat{\underline{q}}_3)$ for $\phi^1_{CDW} = 210^o$, $\phi^2_{CDW} = 330^o$.

Fig. 23 Rotation of ϕ_{Ta} and decrease in magnitude of atomic displacements due to introduction of second harmonic.

Fig. 24 Schematic representation of diffraction intensities along reciprocal lattice vector $\underline{k}$ [10T0] corresponding to the stages shown in Fig. 17a to g. An apparent maxima appears corresponding to an incommensurate superlattice whereas in fact the structures is crystallographically commensurate throughout.

Fig. A.1 Showing that a triplet of CDW having arbitrary phases Φ_i is equivalent to a triplet having equal phases $\Phi_1 = \Phi_2 = \Phi_3$ after an origin shift $\underline{r}'$.

TABLE 1

Comparison of Structure Factors for Commensurate Superlattice Models with Observed Values

hkl	$\|F\|^2(\times 10^{-4})$ $\phi = +90^\circ$	$\phi = -90^\circ$	Moncton et al.
102	0.170	0.178	0.24
104	1.243	1.077	1.26
105	9.193	8.970	9.12
106	2.699	2.713	6.31
107	8.946	8.797	8.32
108	0.008	0.038	0.02
200	1.028	1.042	1.26 (0.55)
201	0.654	0.845	0.50
202	0.110	0.099	0.66
203	3.197	3.767	3.31
205	6.190	6.796	5.89
206	22.326	23.098	23.44
400	22.392	22.260	23.44
401	12.716	9.647	8.91
402	3.706	3.606	3.89
403	15.968	12.738	13.18
500	34.633	34.881	36.31 (33.11)
501	9.616	14.160	14.45
$\bar{1}30$	0.345	0.356	0.54
130	1.603	1.605	1.35
$\bar{1}60$	1.053	0.964	0.52
230	3.049	2.993	4.07
$\bar{2}60$	0.222	0.269	0.60

Values in parantheses represent uncertainties in absolute intensities.

TABLE 2

Code, Fig. numbers and phase shifts of various discommensuration models.

Code	Fig.	$\Delta\Phi_{CDW}{}^{o}$
A1	7	-180
A2	8	-120
A3	9	-60
A4	10	+ 60
A5	11	+120
B1	13	-180
C4	14	+120
C2	15	+ 60

TABLE 3

Parameters p and ϕ_{CDW} and corresponding Fig. numbers for the normal / incommensurate / commensurate state structural transformation.

Fig.	Black Domain		White Domain		R*
	P_1	$\phi_{CDW}{}^{o}$	P_2	$\phi_{CDW}{}^{o}$	
17a	2.0	210	2.3	150	1.00
b	2.3	330	1.6	270	1.88
c	2.6	90	1.3	30	3.50
d	3.0	210	1.0	150	7.00
e	3.3	330	0.6	270	17.00
f	3.6	90	0.3	30	71.00
g	4.0	210	-	-	-

*R = $\frac{\text{Area of (anharmonically) favoured structure}}{\text{Area of unfavoured structure}}$

= $(8/p_2^2) - 1$

APPENDIX I

Phase Relationship for CDW Triplets After Origin Shift

Consider Fig. A 1 where $\underline{q}_i$ (i = 1,2,3) represent three CDW vectors referred to origin 0. Suppose they have equal amplitudes but arbitrary phases Φ_i. An indistinguishable electron density distribution may be generated using CDW triplets $\underline{q}_i'$, having identical amplitudes (or wavelengths λ), but with three identical phases $\Phi_i' = \Phi'$ referred to an origin 0' displaced by vector $\underline{r}'$ from 0. We require

$$\Phi' = \Phi_1 + \underline{q}_1 \cdot \underline{r}' = \Phi_2 + \underline{q}_2 \cdot \underline{r}' + 2m\pi = \Phi_3 + \underline{q}_3 \cdot \underline{r}' + 2n\pi \qquad (A.1)$$

where m, n are integers. To find $\underline{r}'$ we put

$$\underline{r}' = x\lambda\hat{\underline{q}}_1 + y\lambda\hat{\underline{q}}_2 \qquad (A.2)$$

where x and y are to be determined, and $\hat{\underline{q}}_i$ are unit vectors parallel to $\underline{q}_i$. Then from (A.1)

$$\Phi_1 + 2\pi(x - y/2) = \Phi_2 + 2\pi(-x/2 + y) + 2m\pi$$
$$= \Phi_3 + 2\pi(-x/2 - y/2) + 2n\pi \qquad (A.3)$$

yielding

$$x = [\Phi_3 - \Phi_1 + 2n\pi]/3\pi$$
$$y = [\Phi_3 - \Phi_2 + 2(n-m)]/3\pi \qquad (A.4)$$

and

$$\Phi' = (\Phi_1 + \Phi_2 + \Phi_3)/3 + (2\pi/3)(n+m) \qquad (A.5)$$

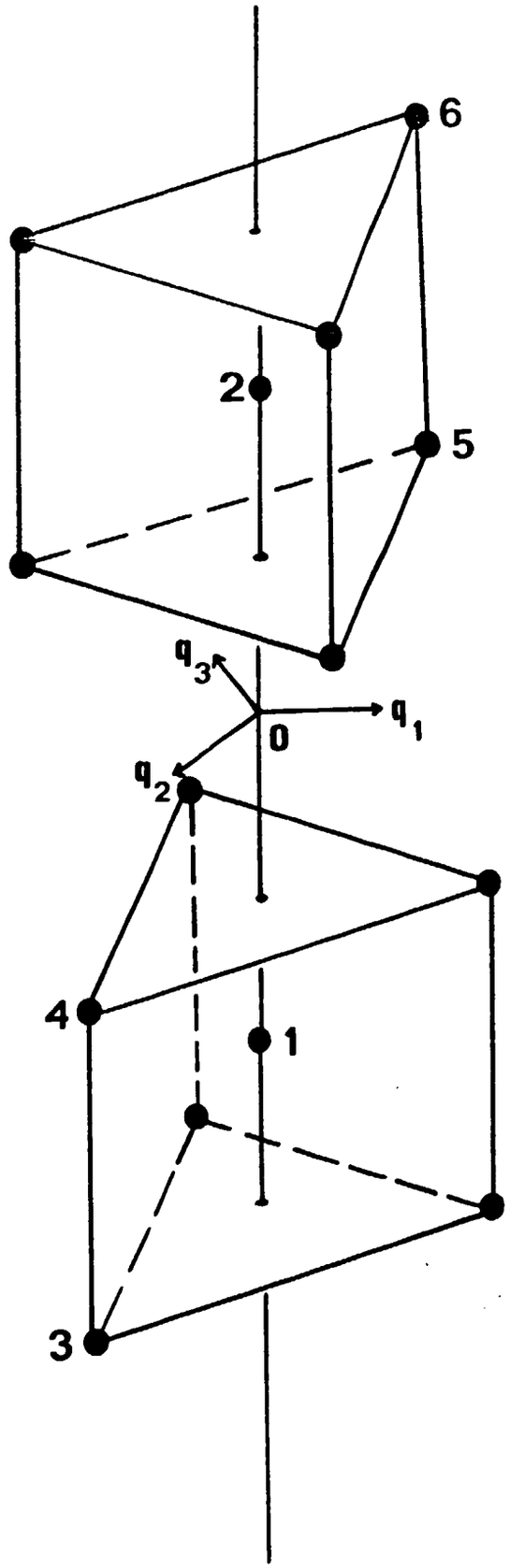
6
2
5
q_3
q_1
0
q_2
4
1
3

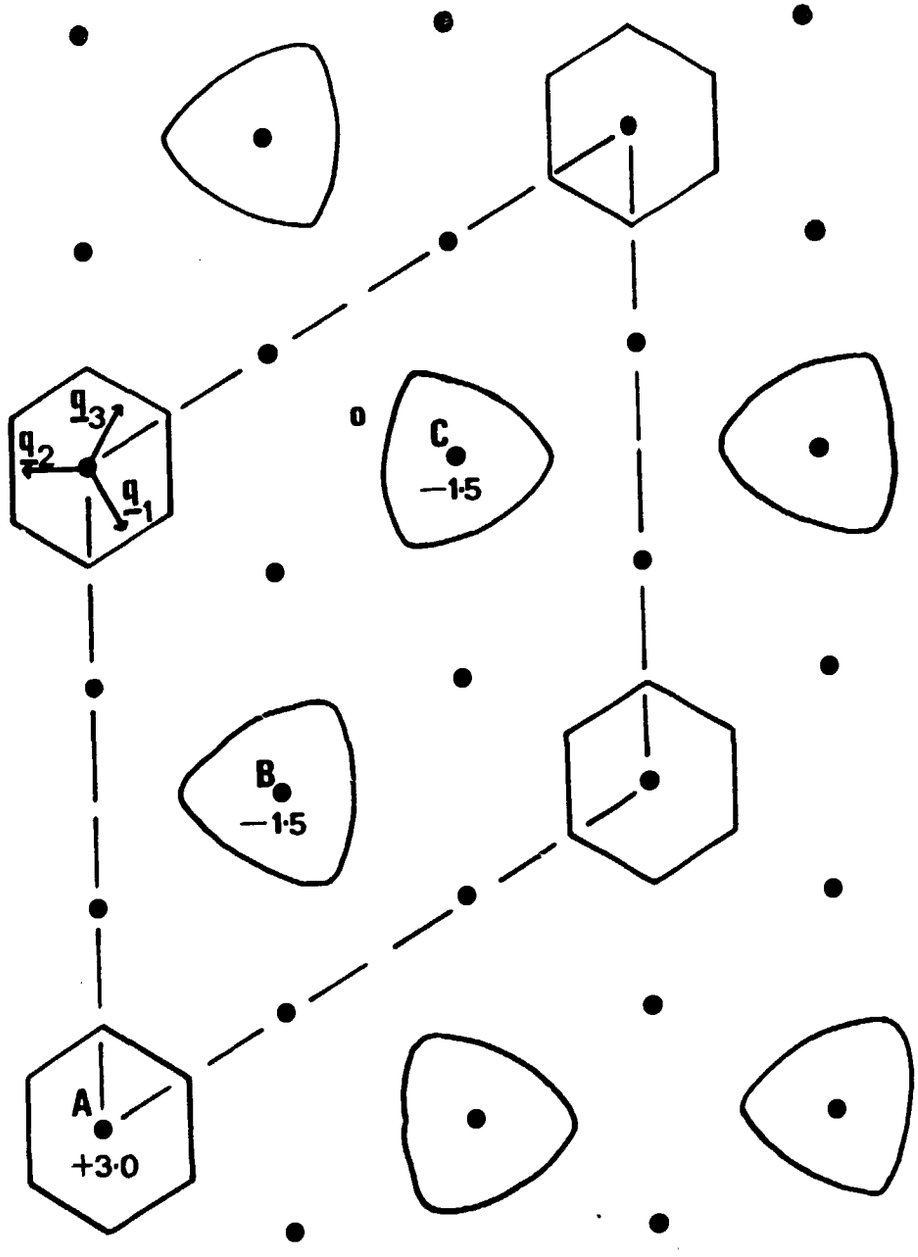

FIG 2

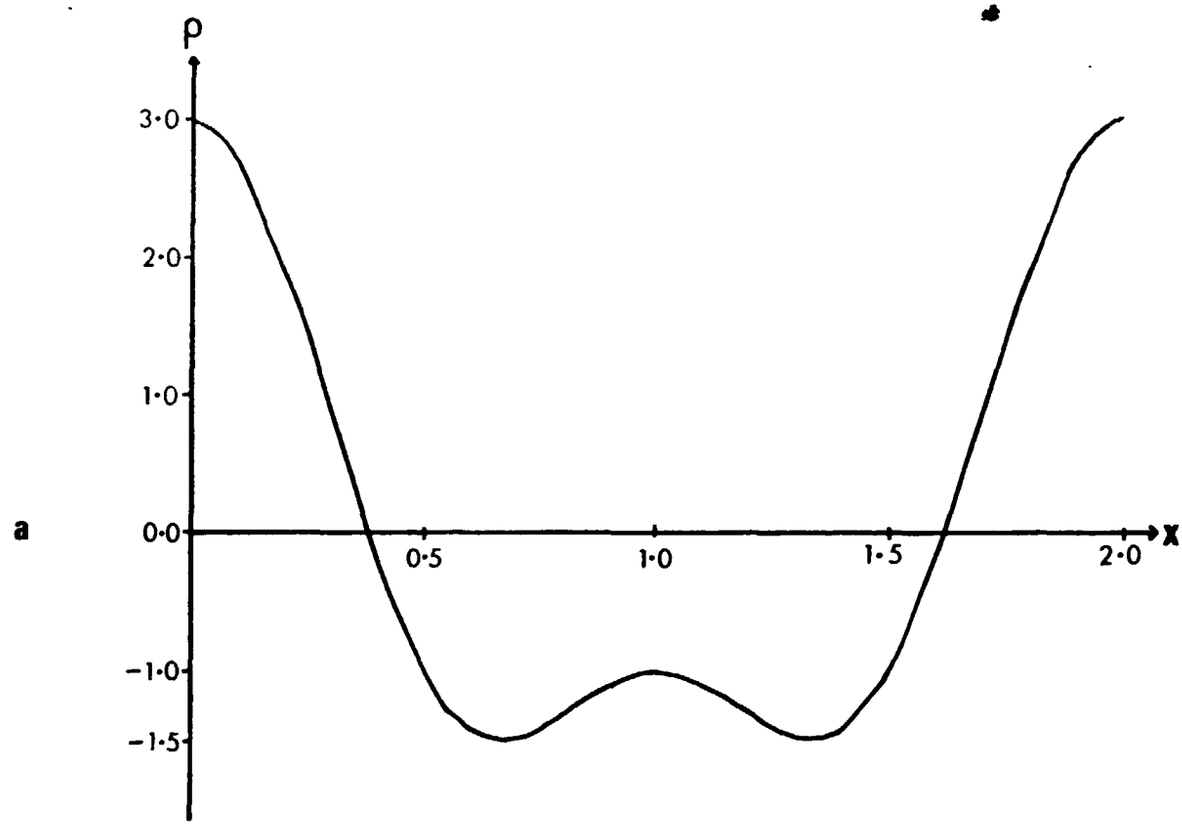
a
ρ
3·0
2·0
1·0
0·0
−1·0
−1·5
0·5
1·0
1·5
2·0
X

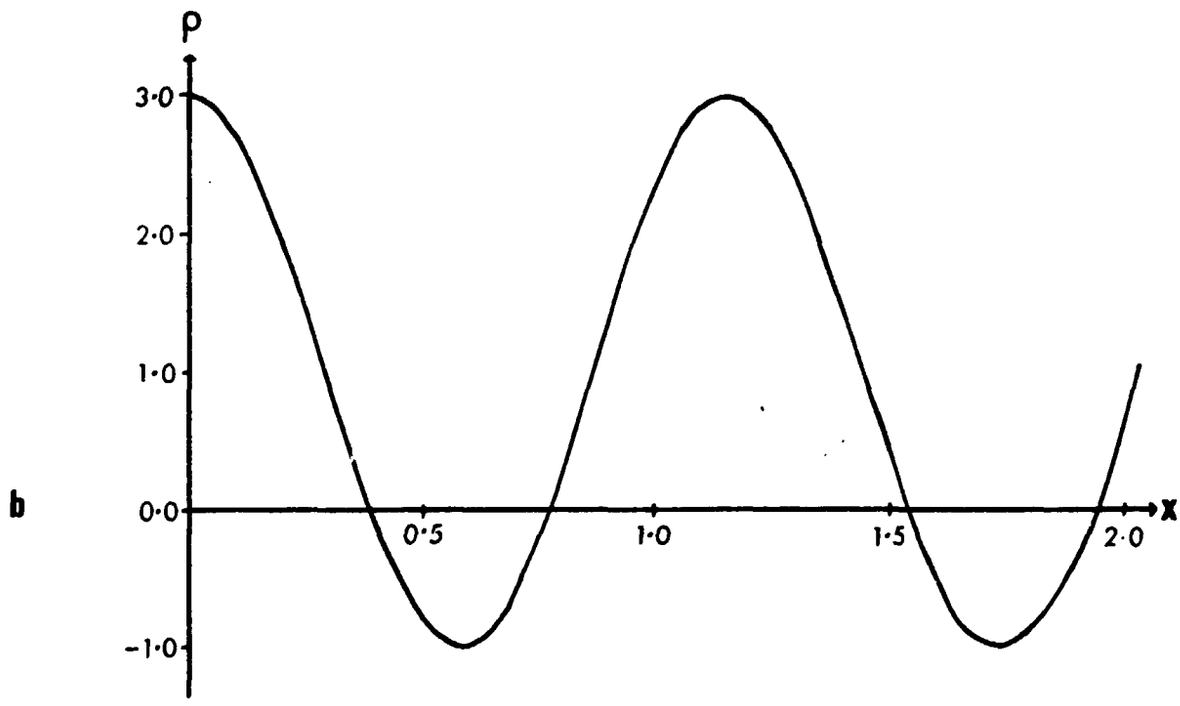
b
ρ
3·0
2·0
1·0
0·0
−1·0
0·5
1·0
1·5
2·0
X

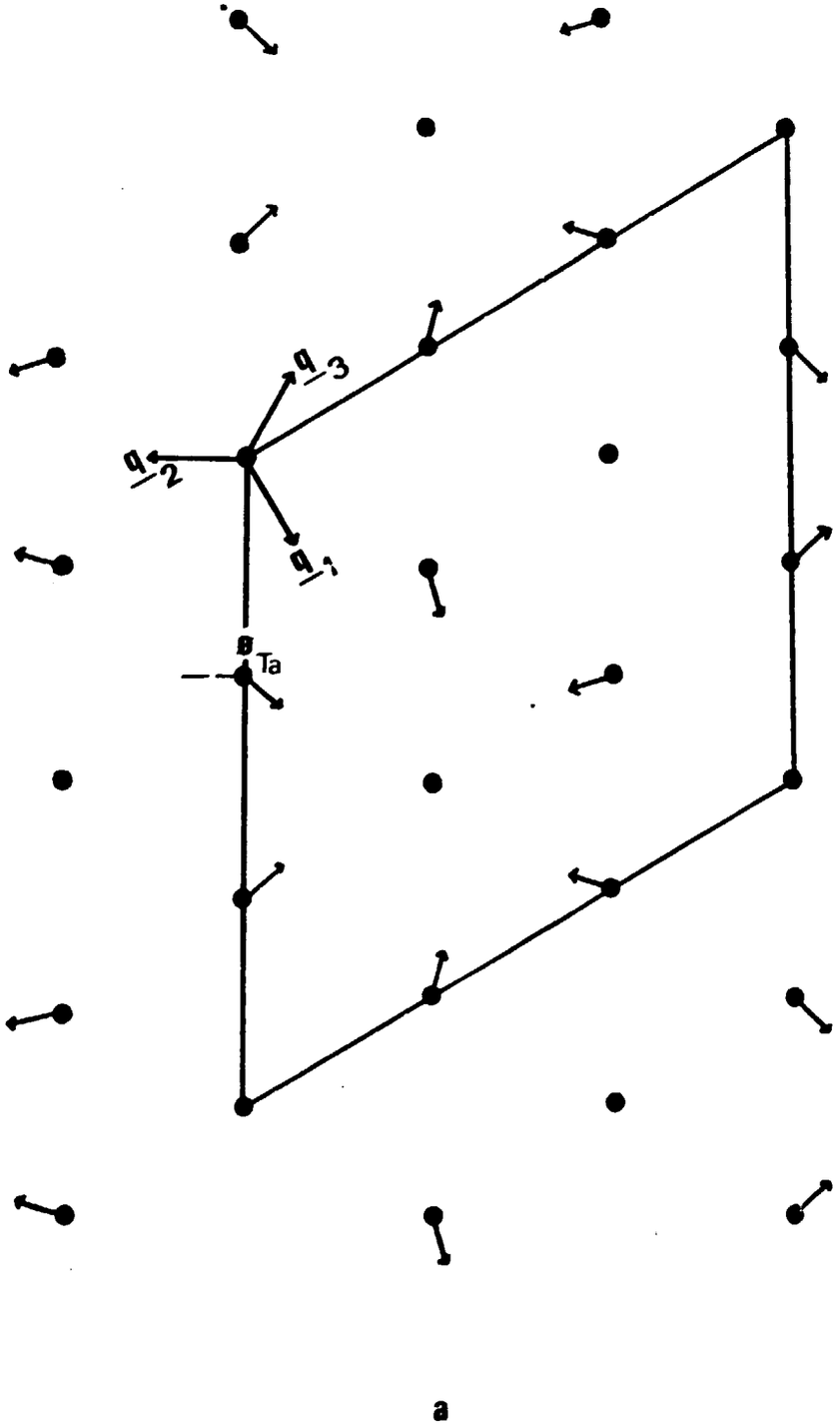

FIG 4

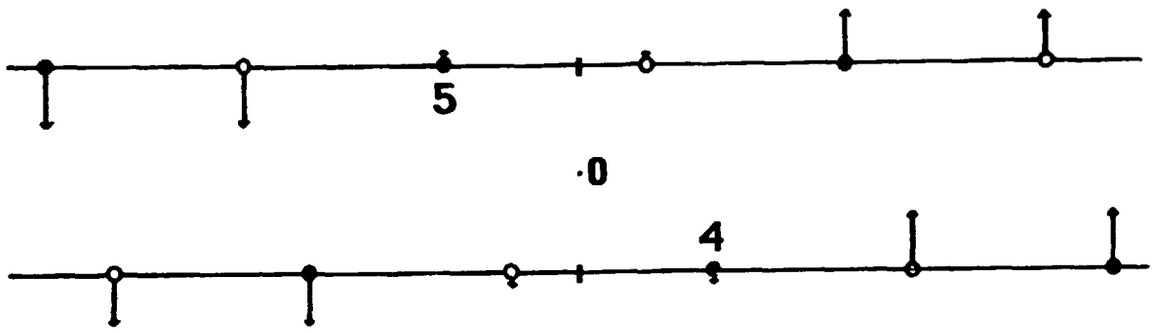

b

FIG 4

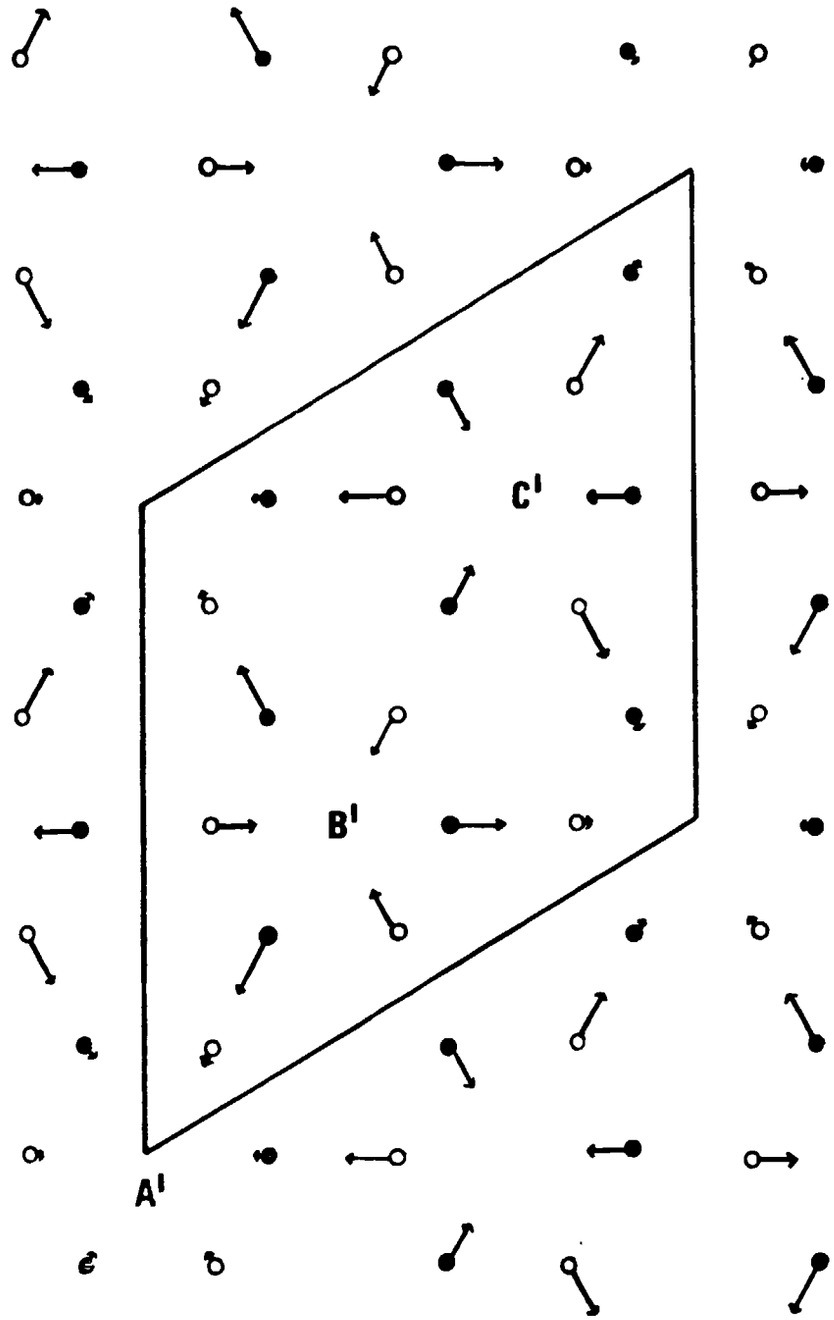

C

FIG 4

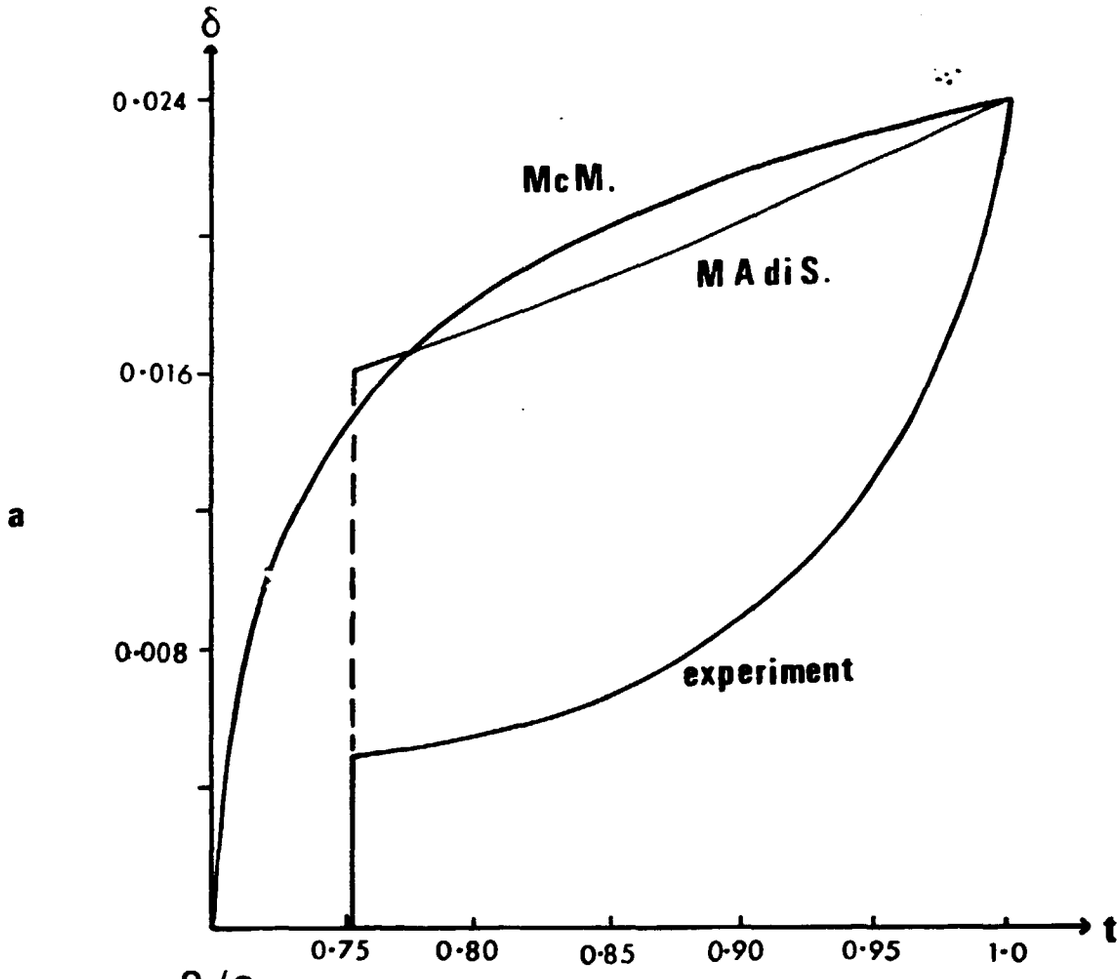
δ
0·024
0·016
0·008
McM.
MAdiS.
experiment
0·75
0·80
0·85
0·90
0·95
1·0
t

a

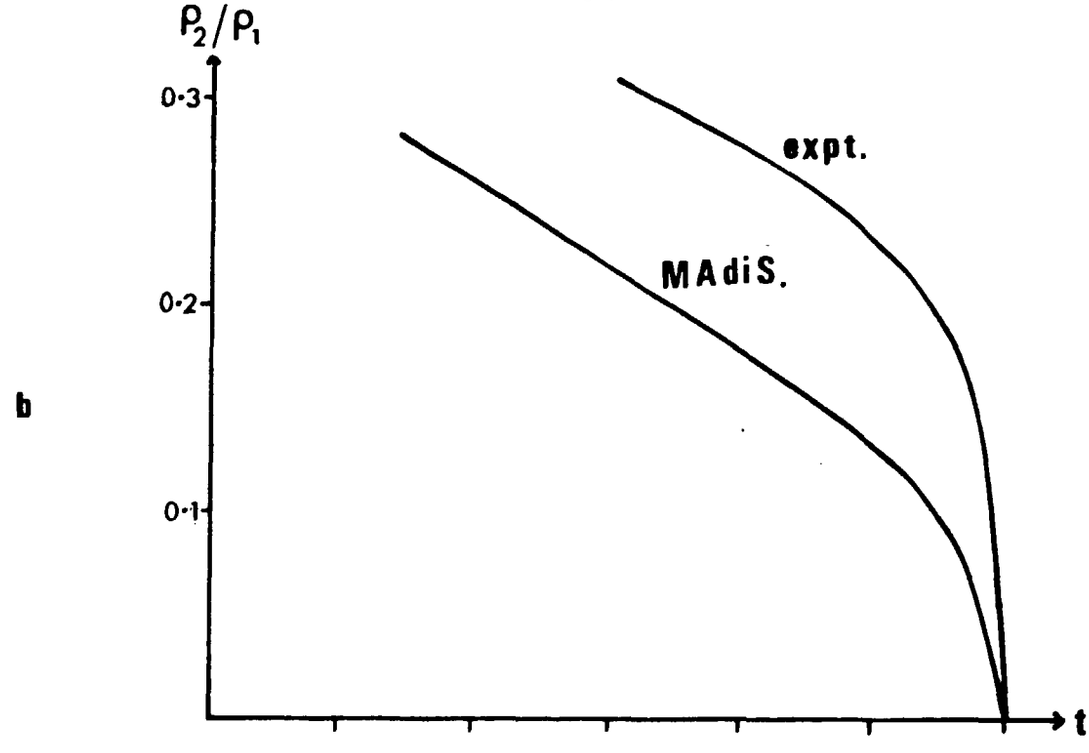
ρ2/ρ1
0·3
0·2
0·1
expt.
MAdiS.
t

b

FIG 5

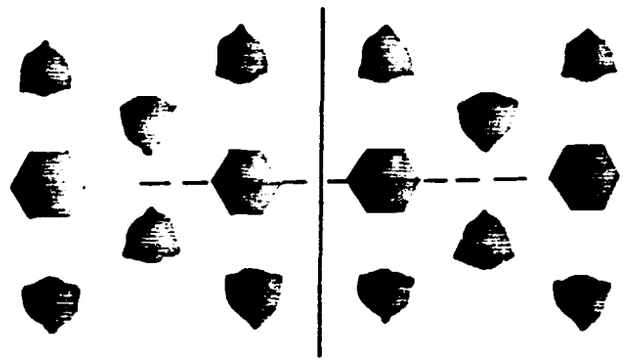

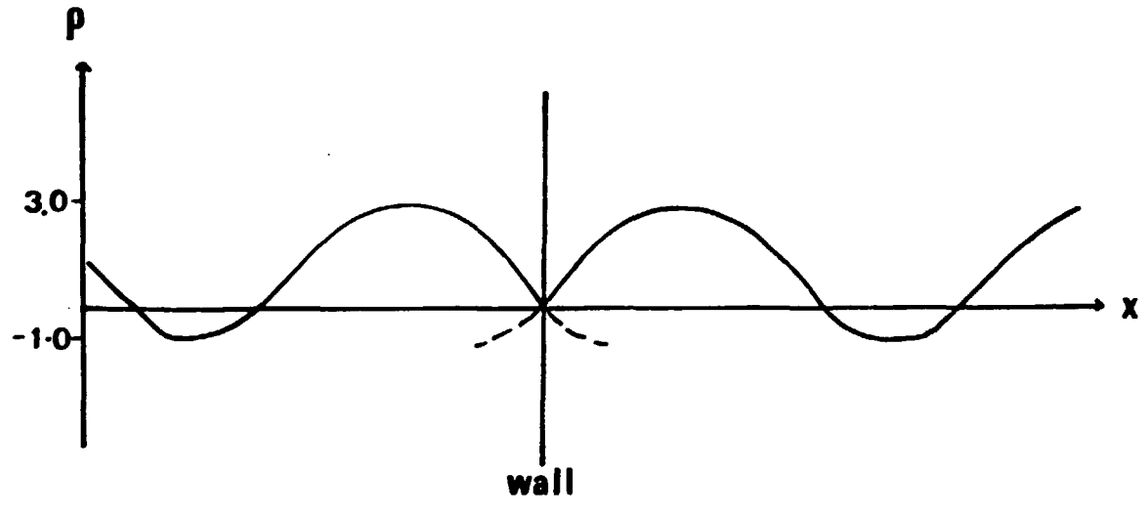

FIG 6

A1

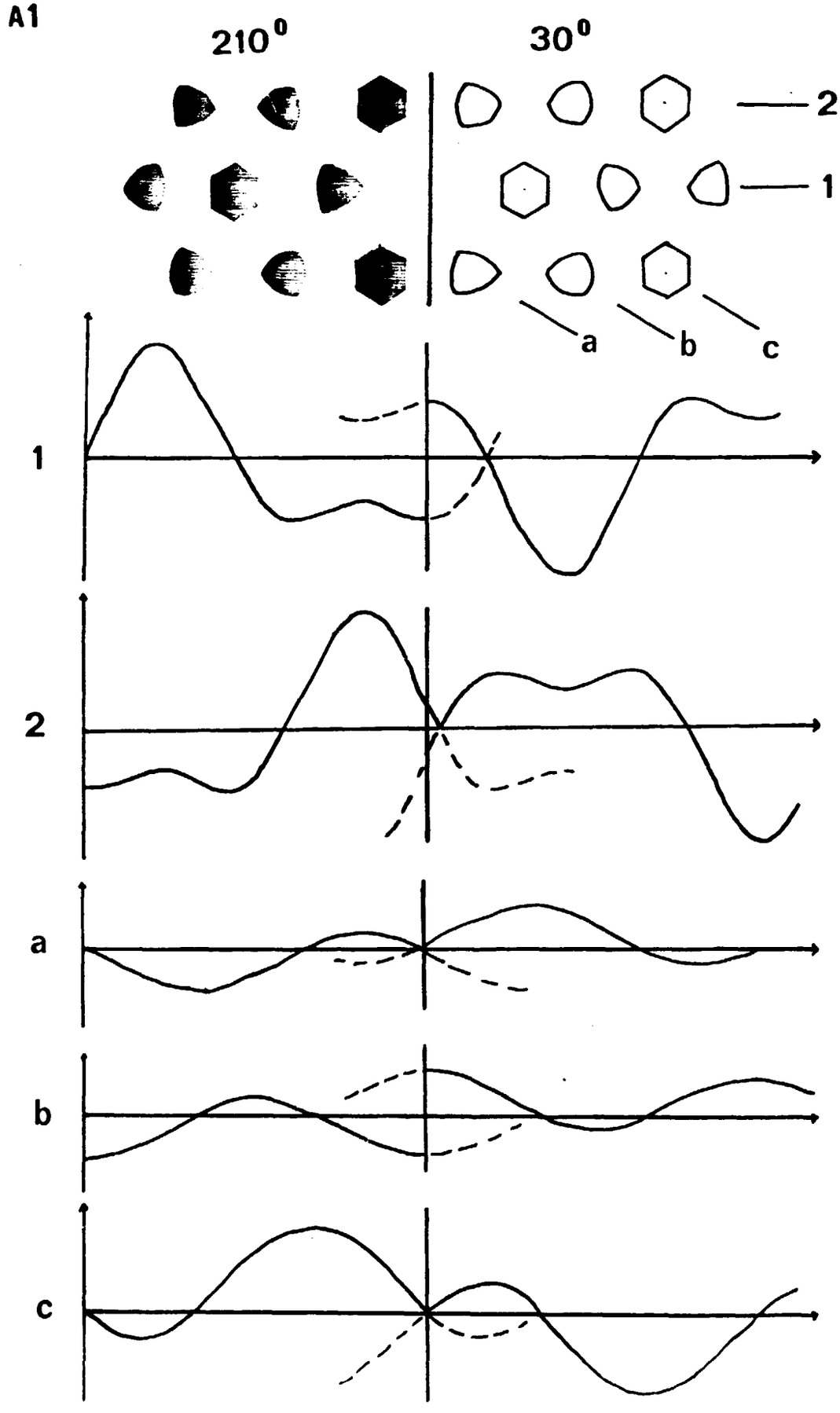

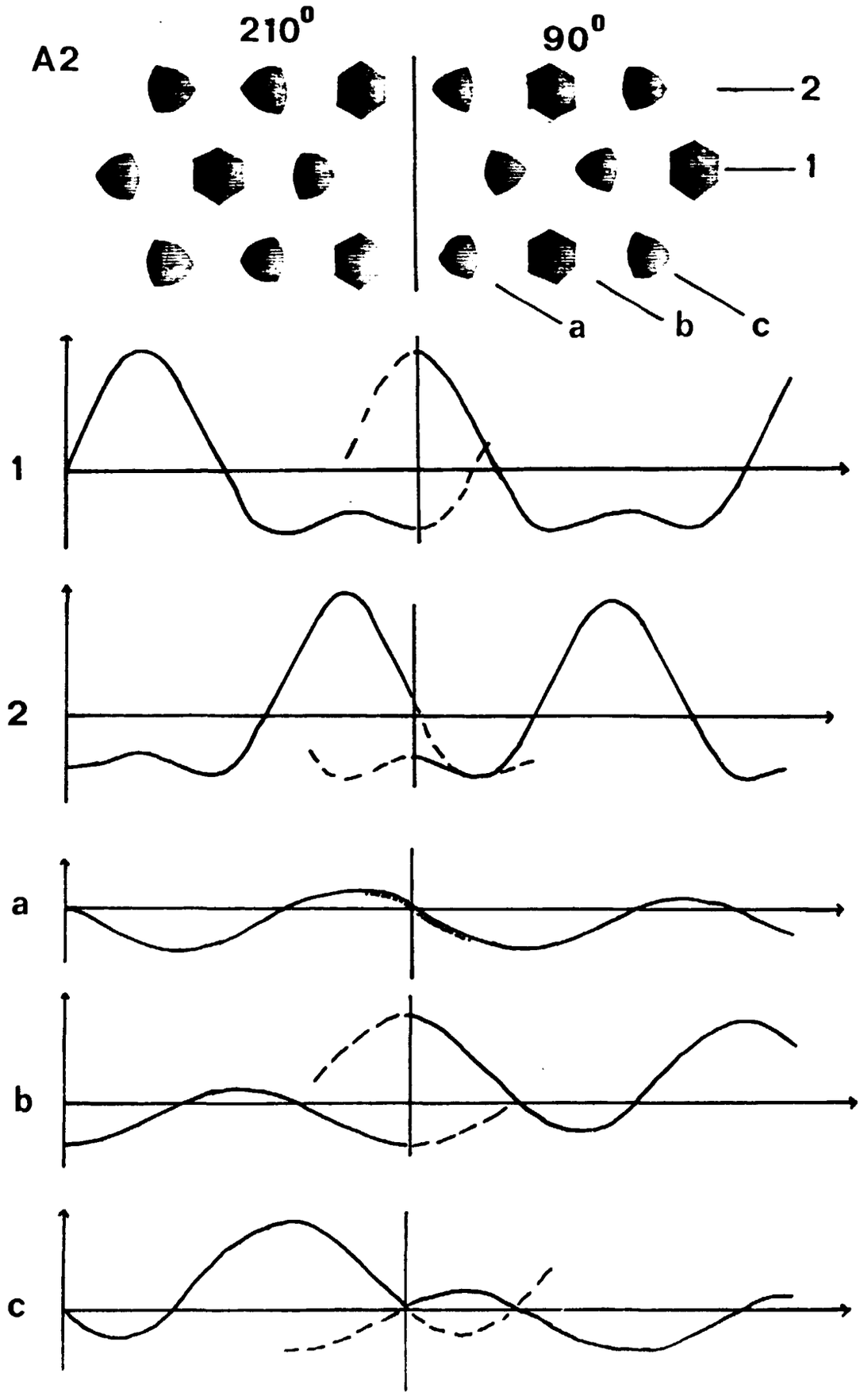
A2
210°
90°
2
1
a
b
c
1
2
a
b
c

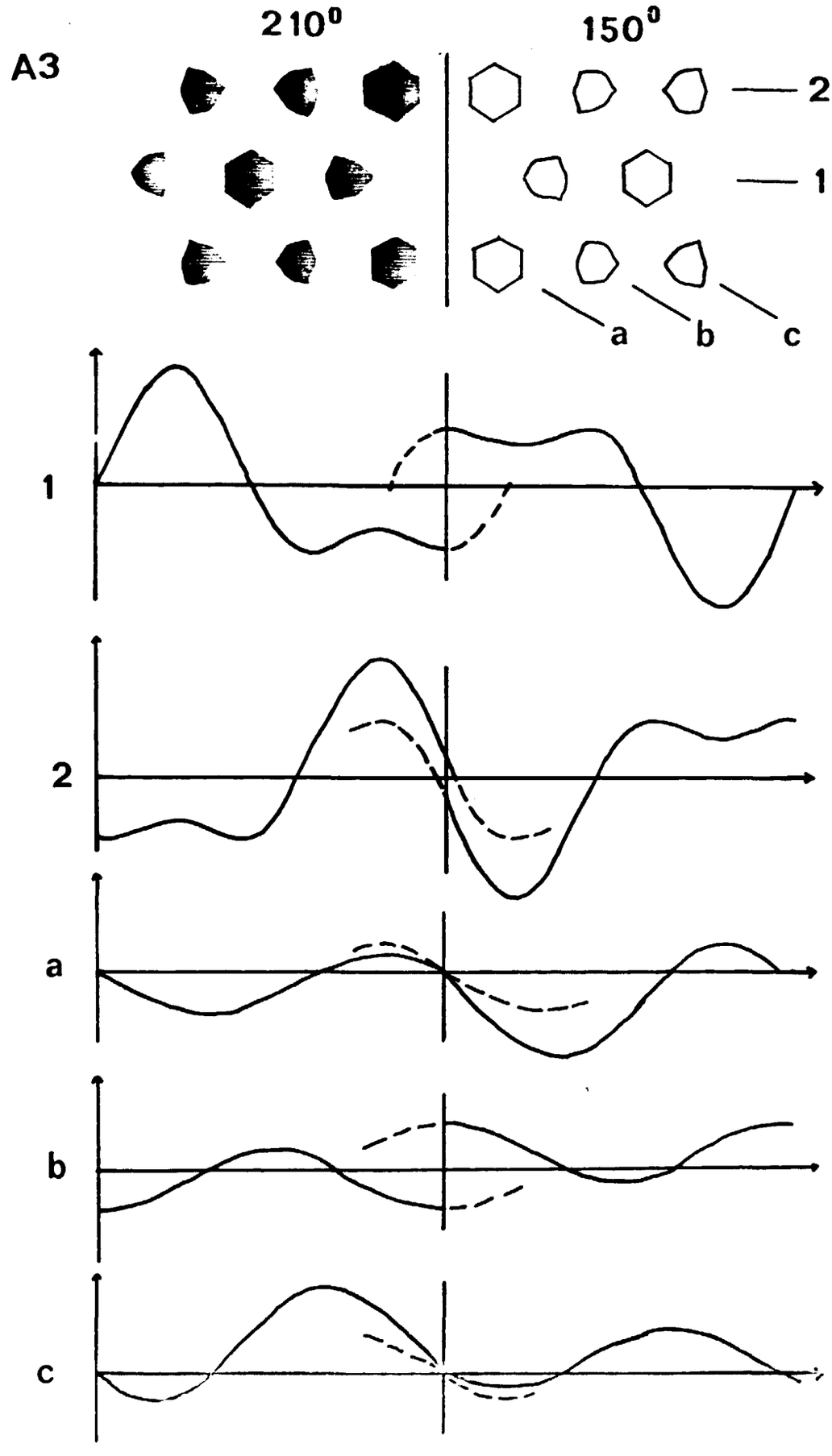
A3
210⁰
150⁰
2
1
a
b
c
1
2
a
b
c

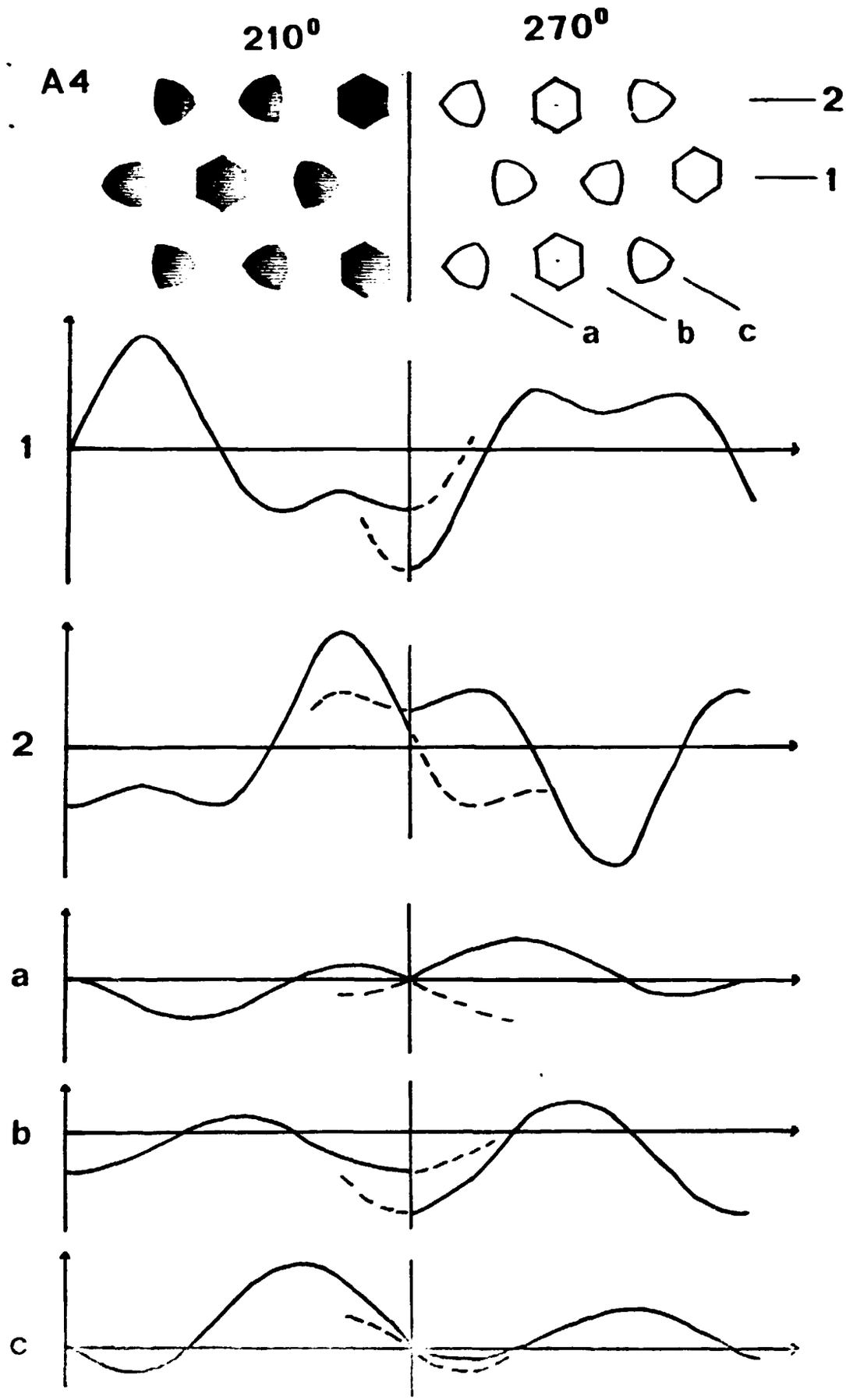
210⁰
270⁰
A4
2
1
a
b
c
1
2
a
b
c

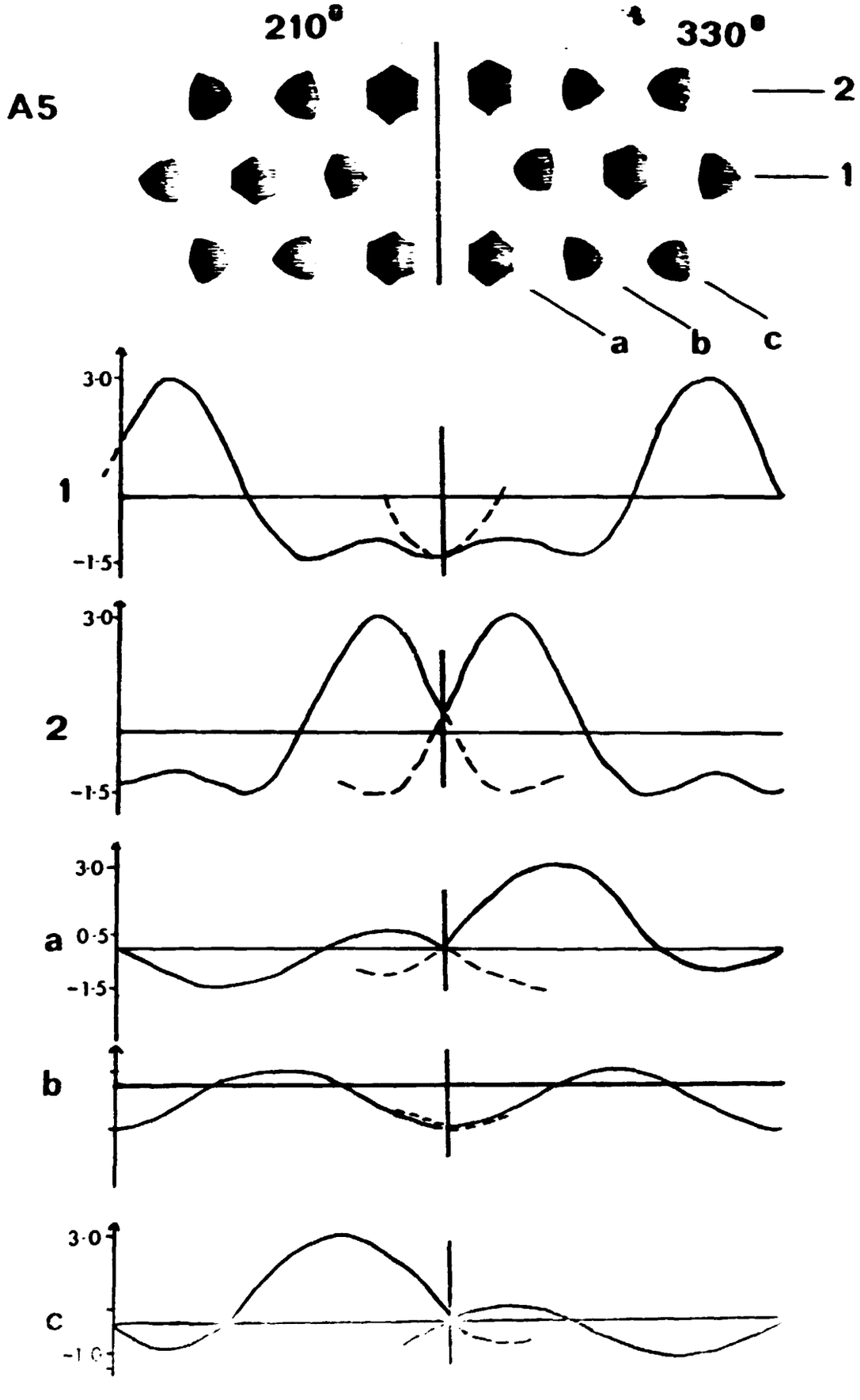
210°
330°
A5
2
1
a
b
c
3·0
1
-1·5
3·0
2
-1·5
3·0
a
0·5
-1·5
b
3·0
c
-1·0

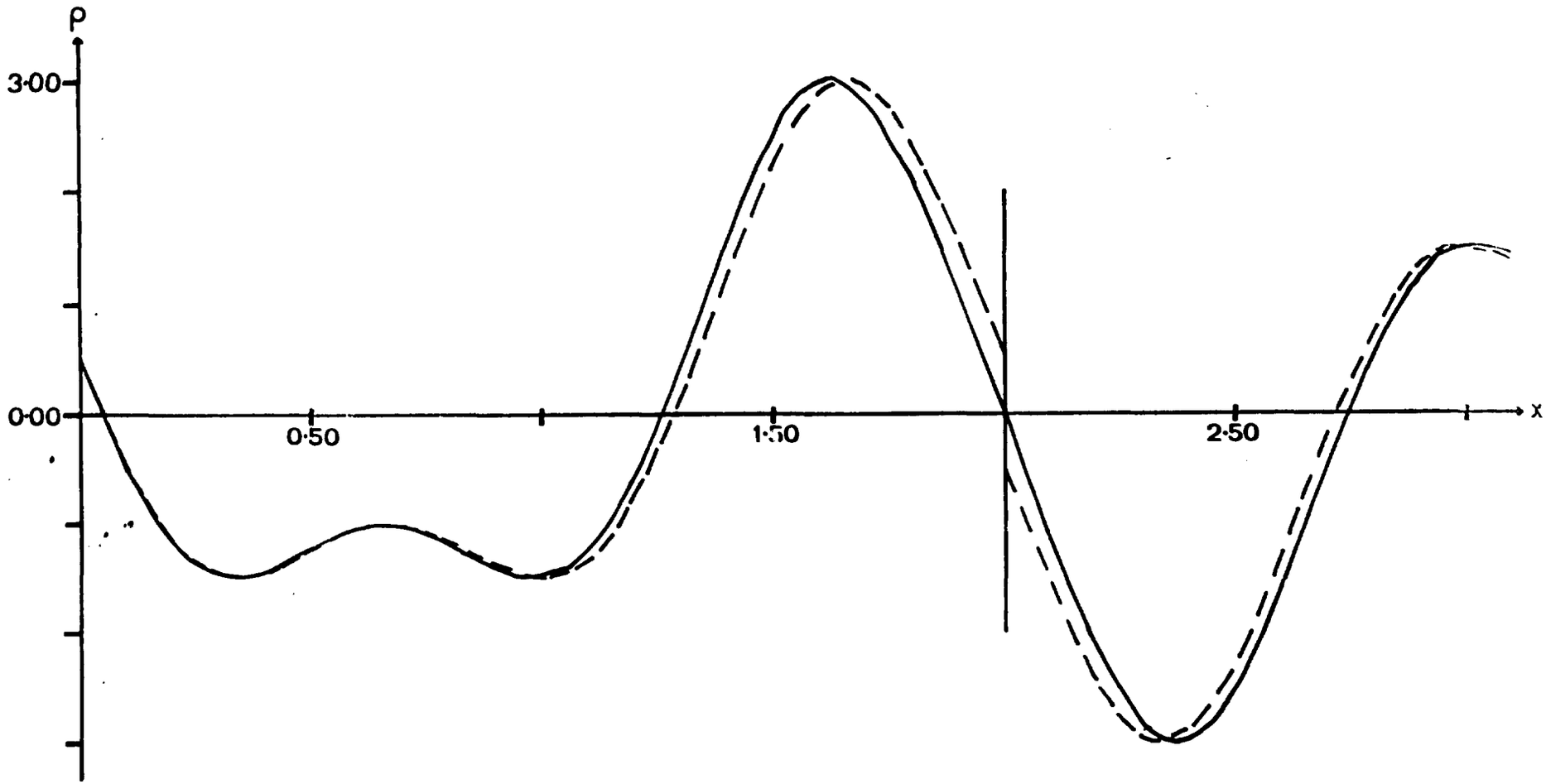

a

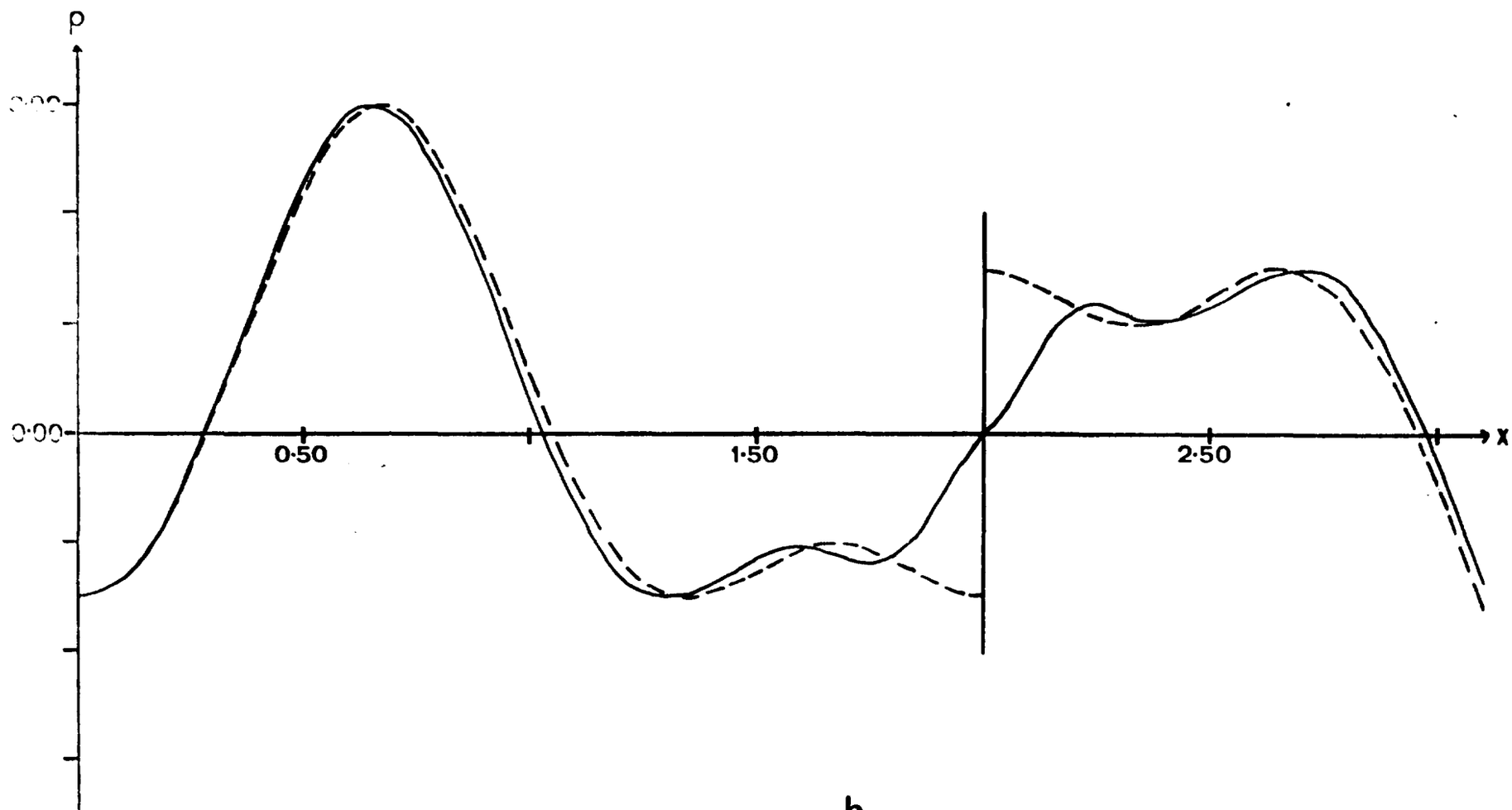

b

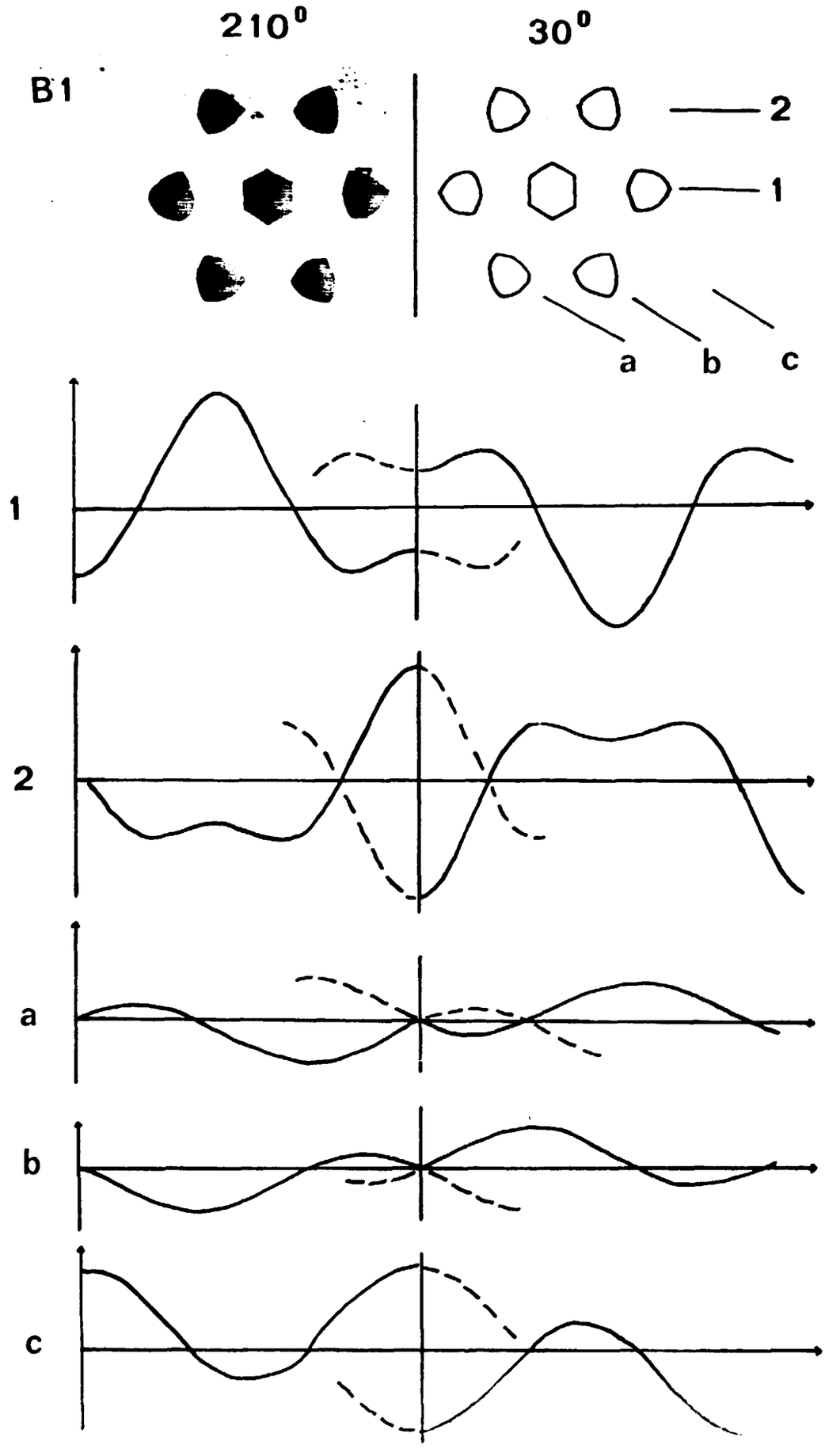
210⁰
30⁰
B1
2
1
a
b
c
1
2
a
b
c

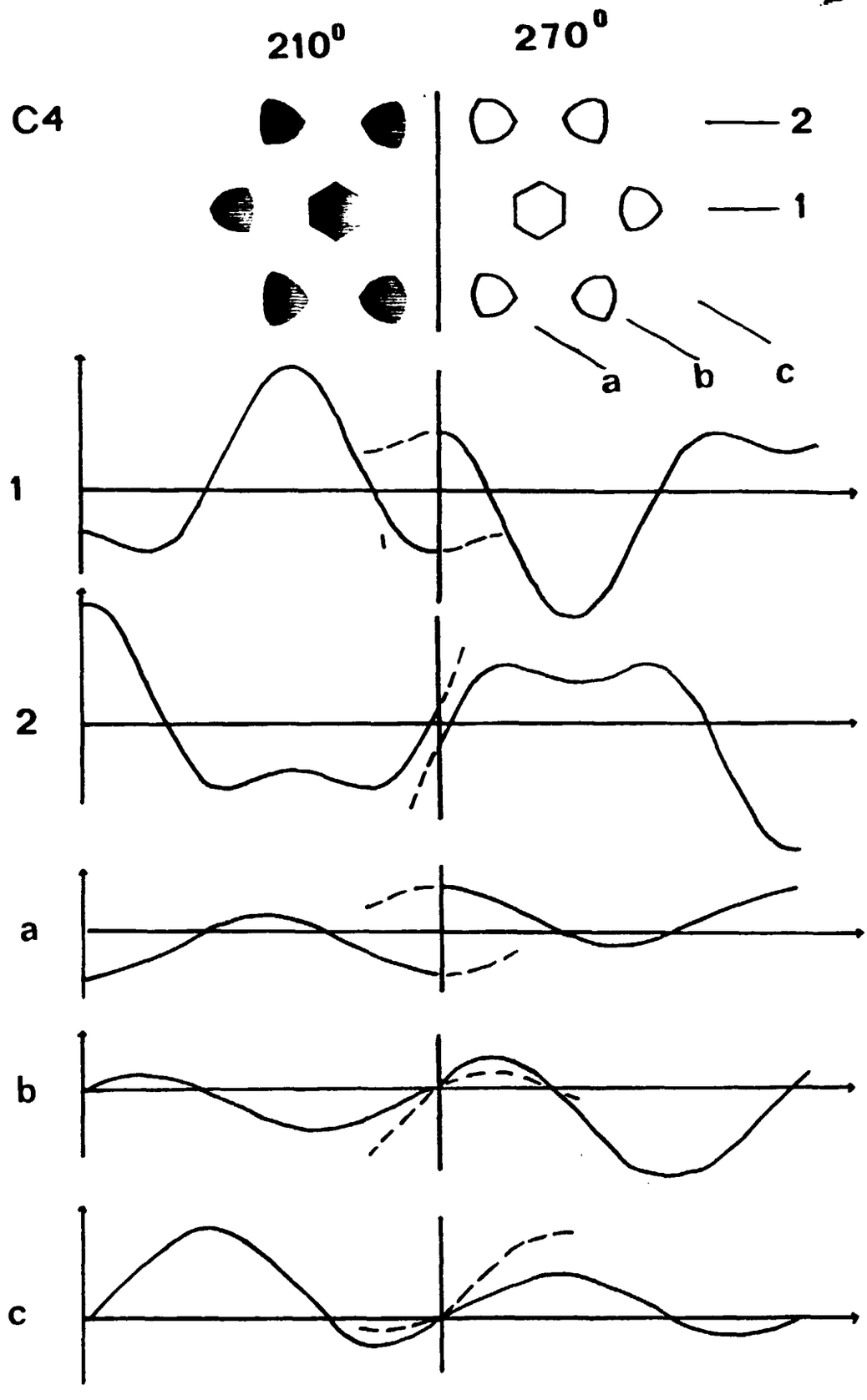
210⁰
270⁰
C4
2
1
a
b
c
1
2
a
b
c

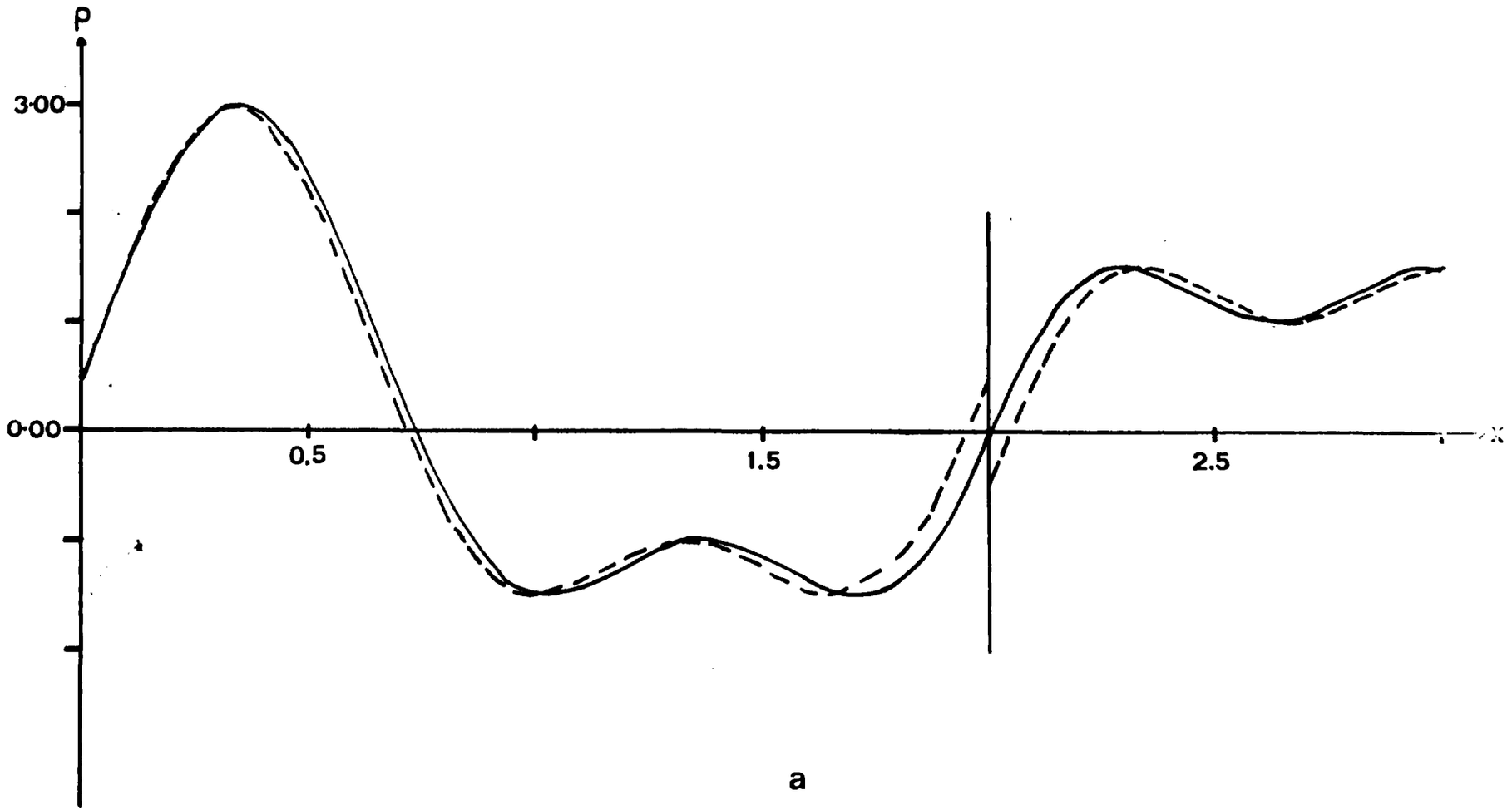

a

0·00
3·00
p
0·50
1·50
2·50
q

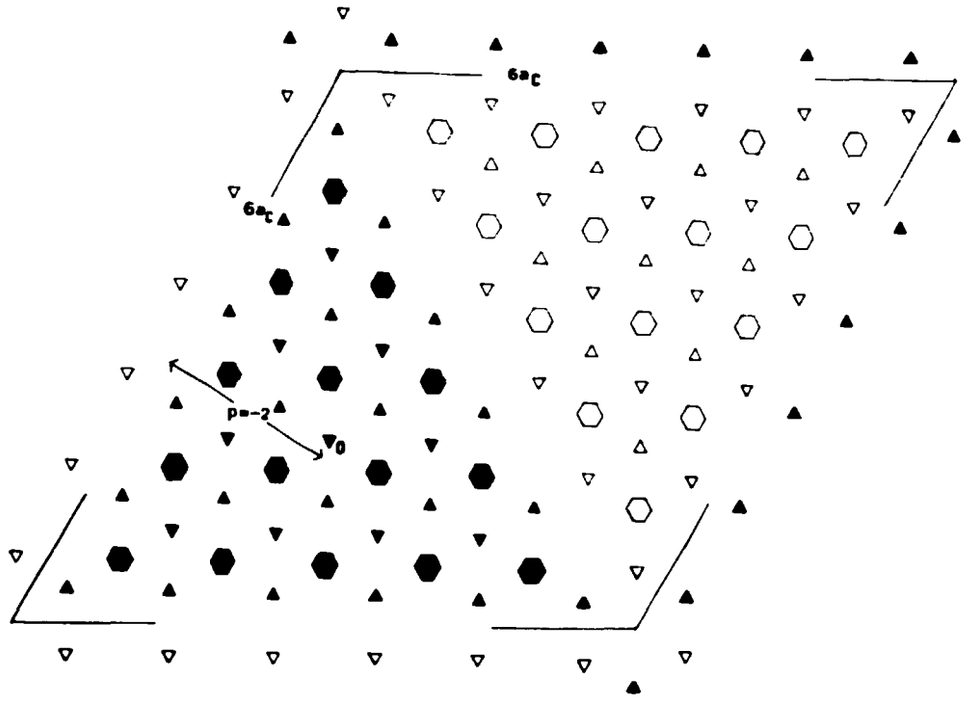

a

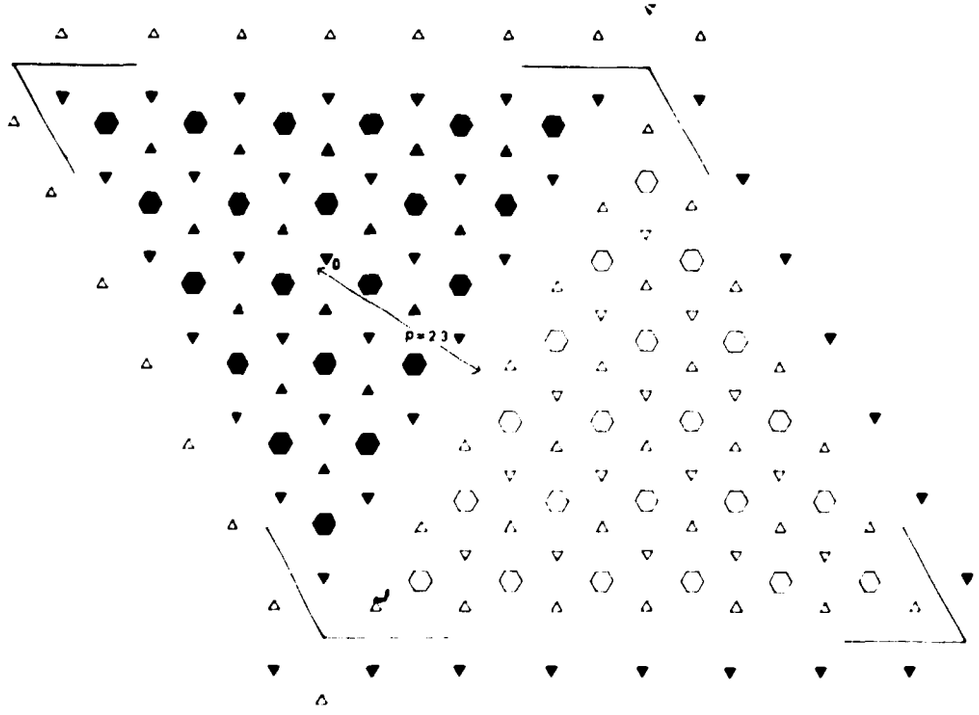

b

FIG 16

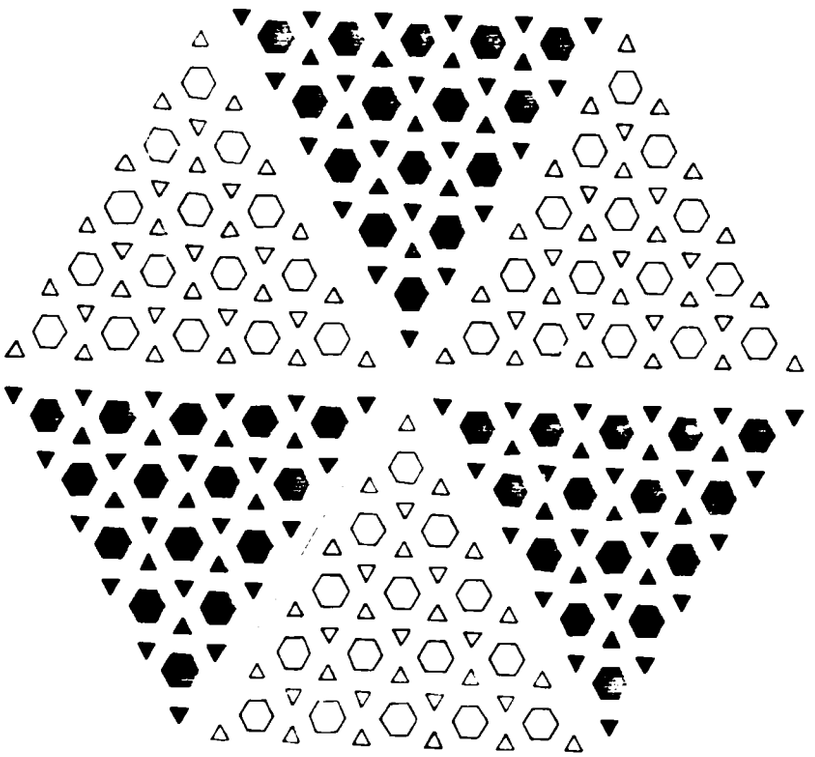

a

FIG 17

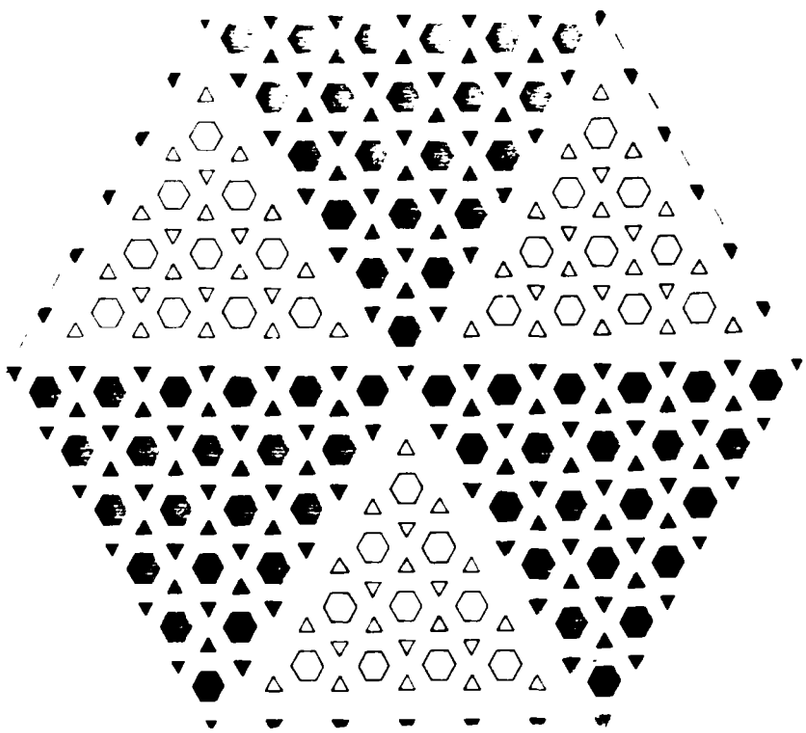

b

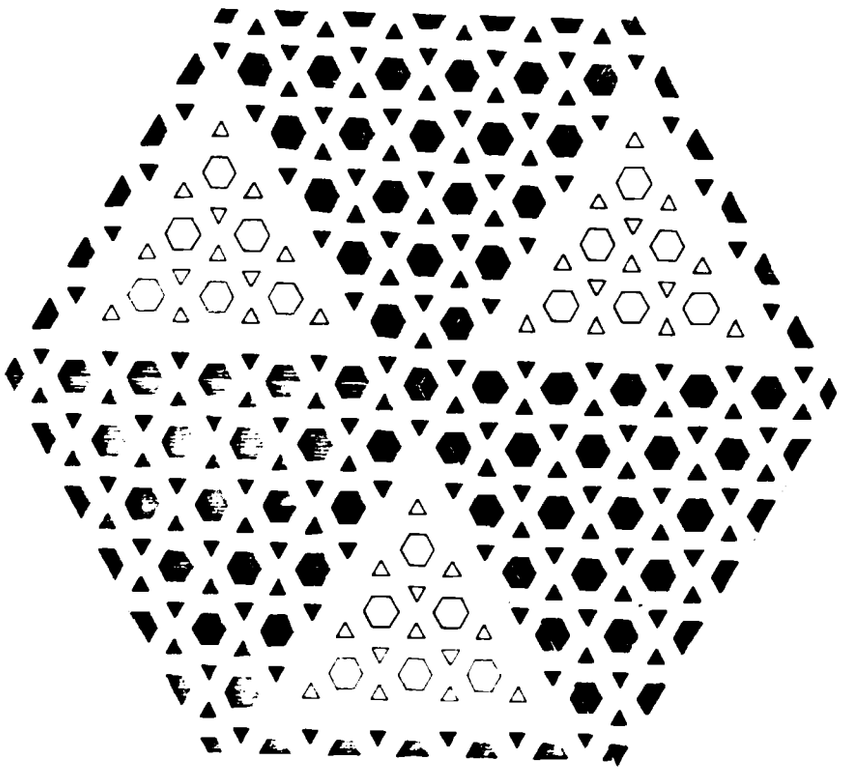

C

FIG 7

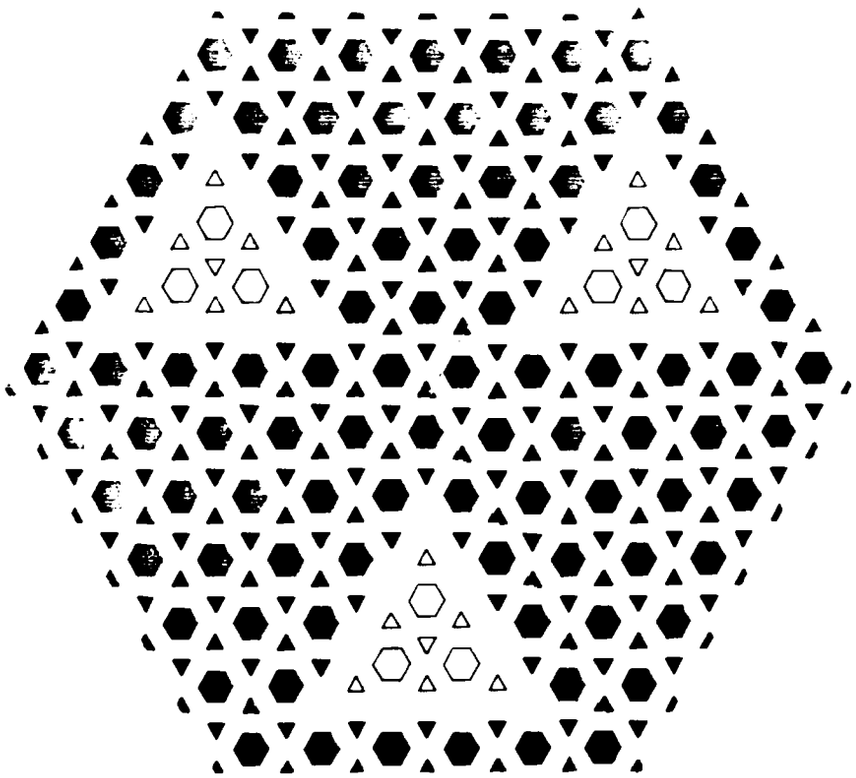

d

FIG 17

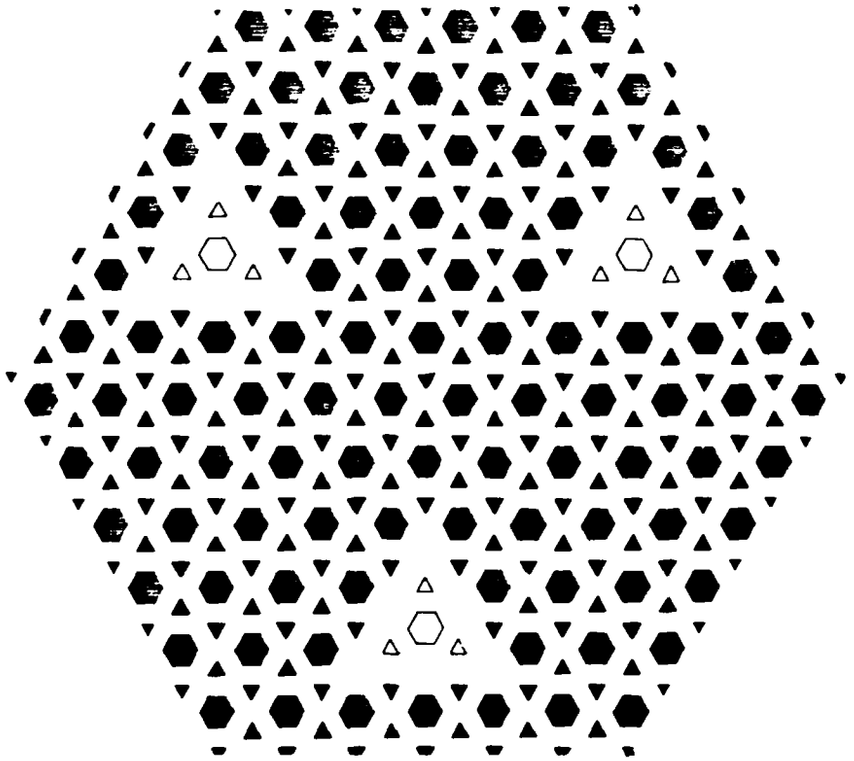

e

FIG 17

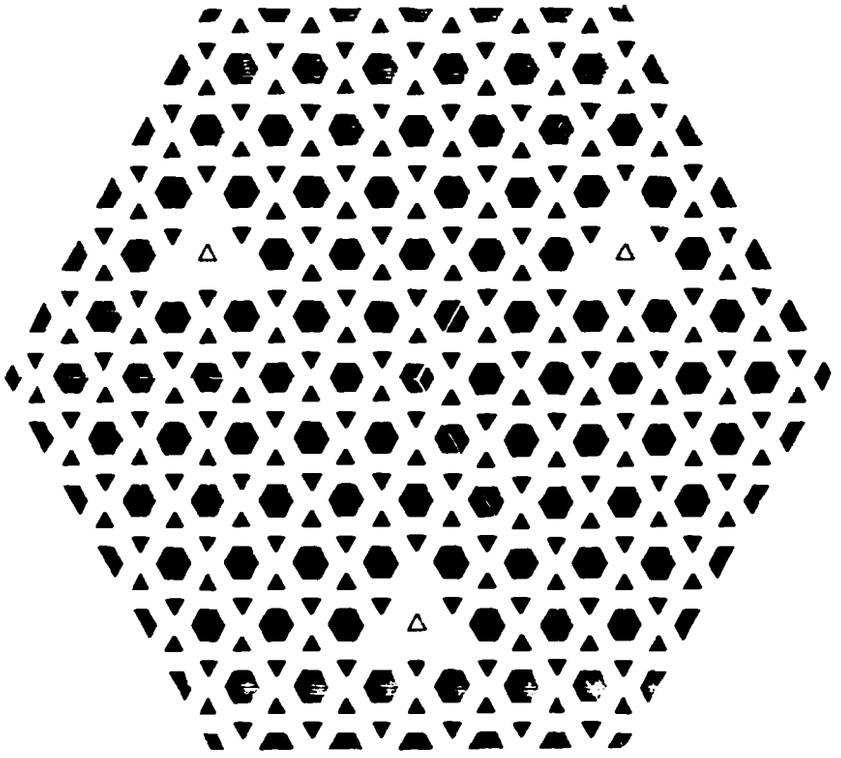

f

FIG 17

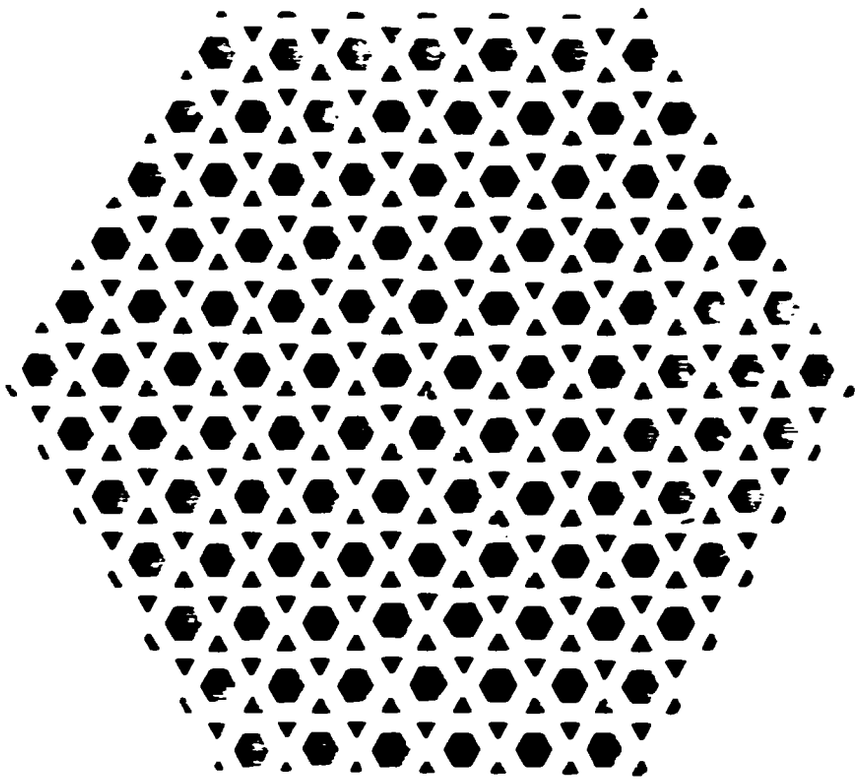

g

Fig 12

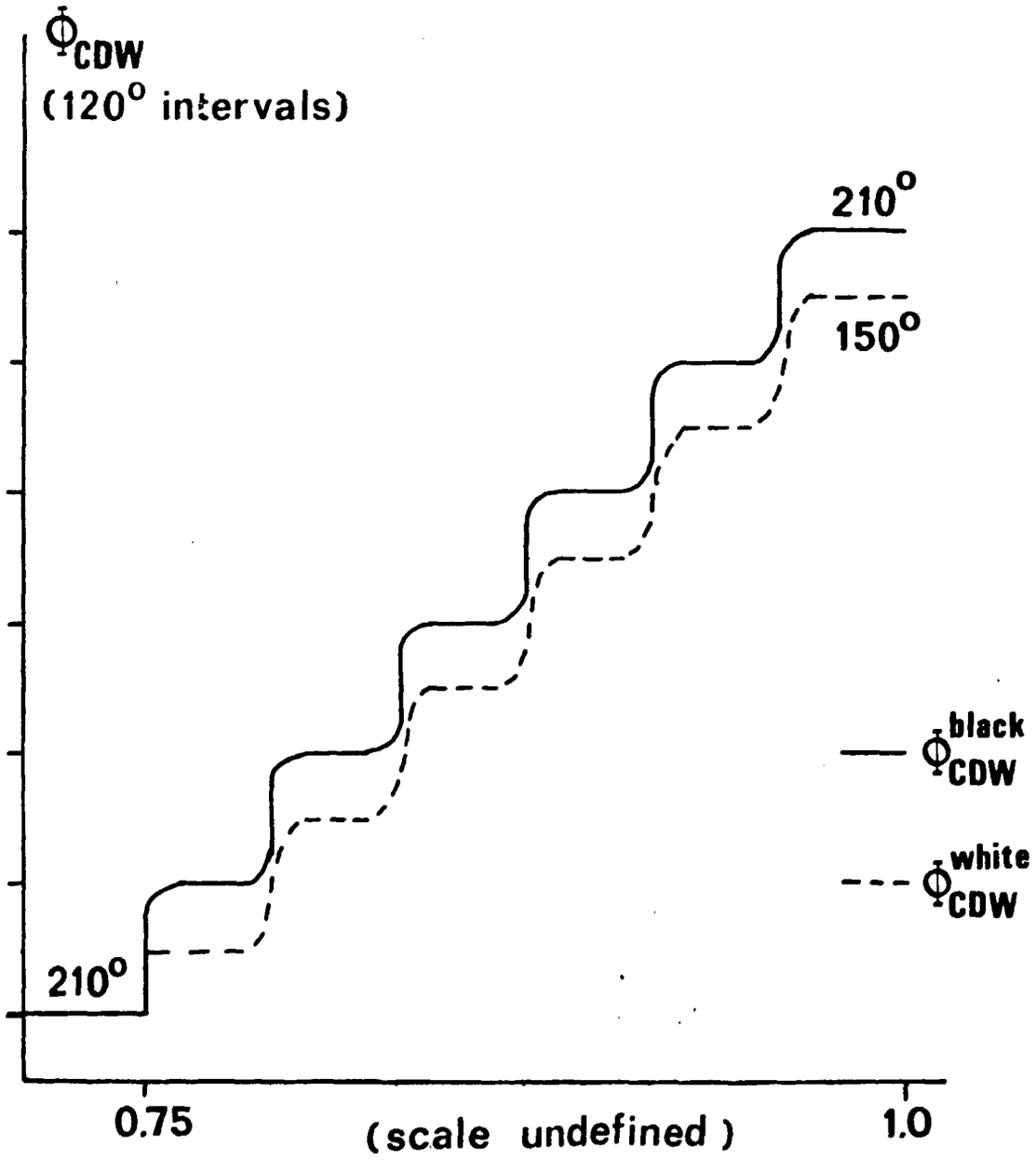
Φ_{CDW}
(120° intervals)
210°
150°
210°
Φ^{black}_{CDW}
Φ^{white}_{CDW}
0.75
(scale undefined)
1.0

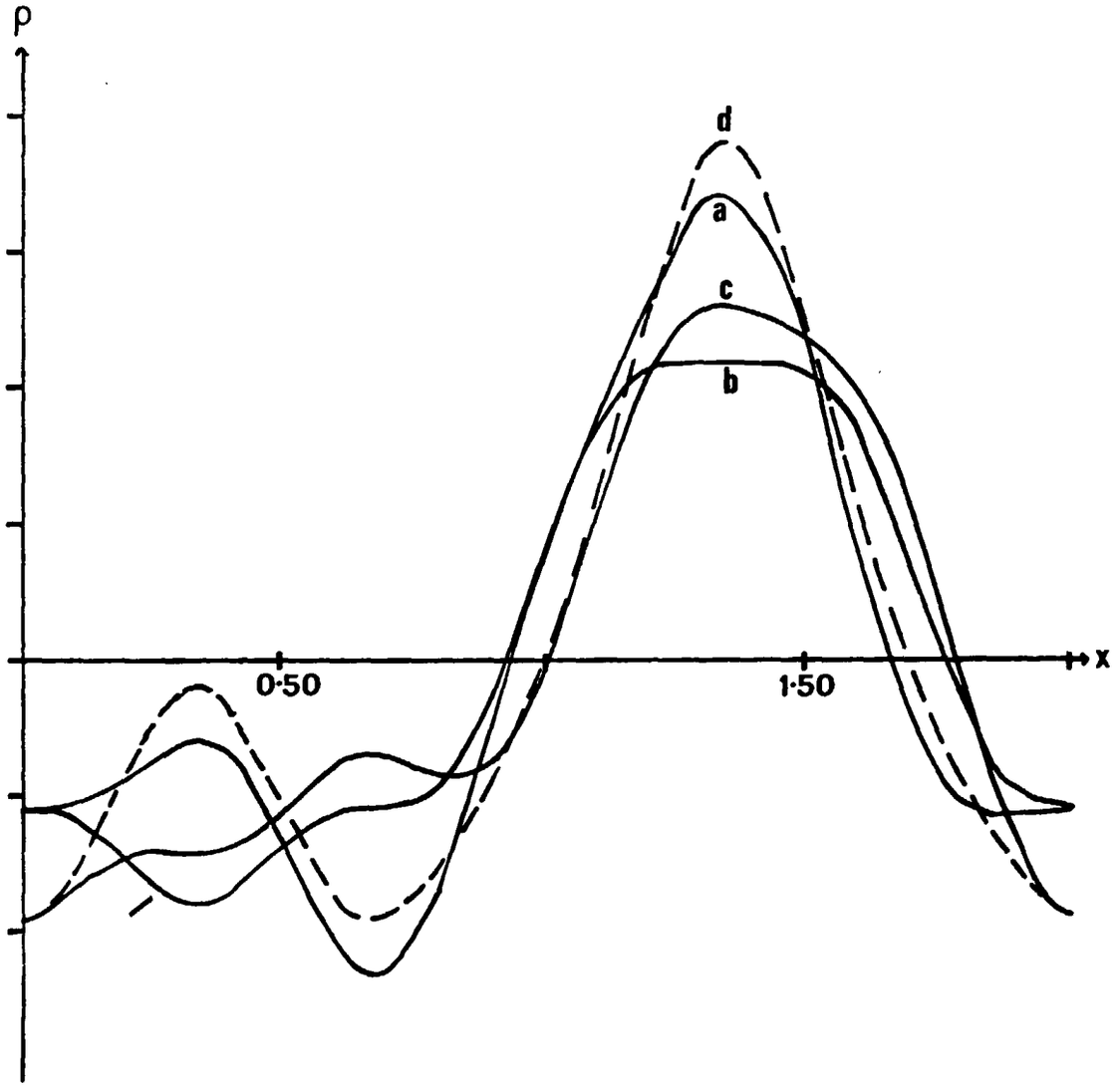

FIG 19

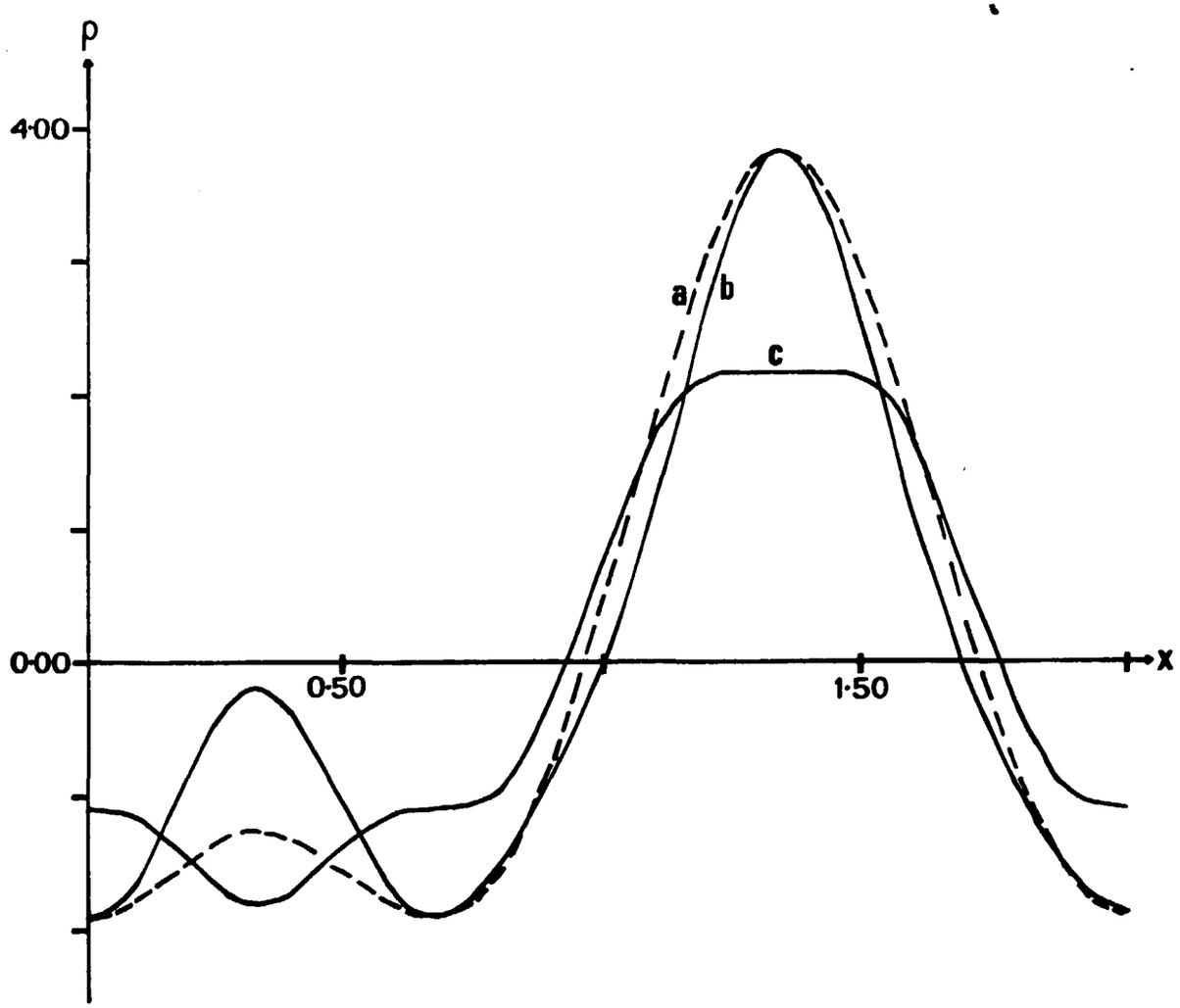

FIG 20

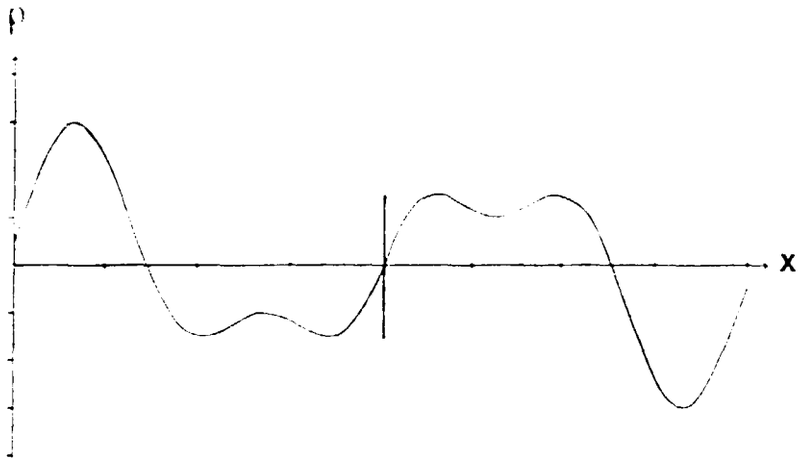

δ=0.024

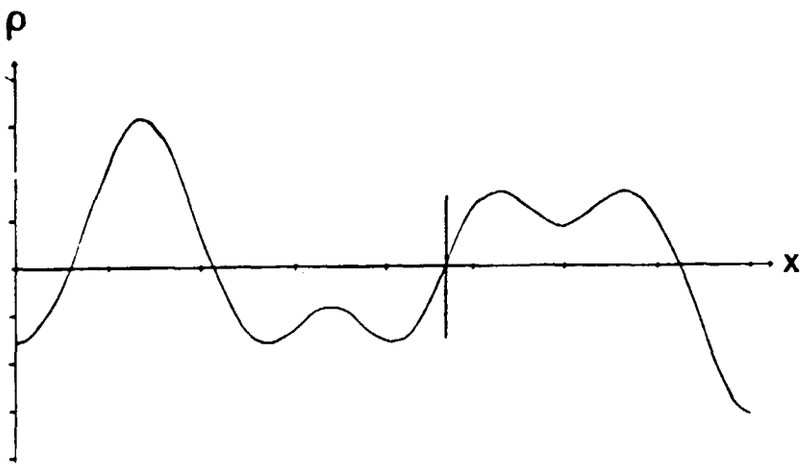

δ=0.020

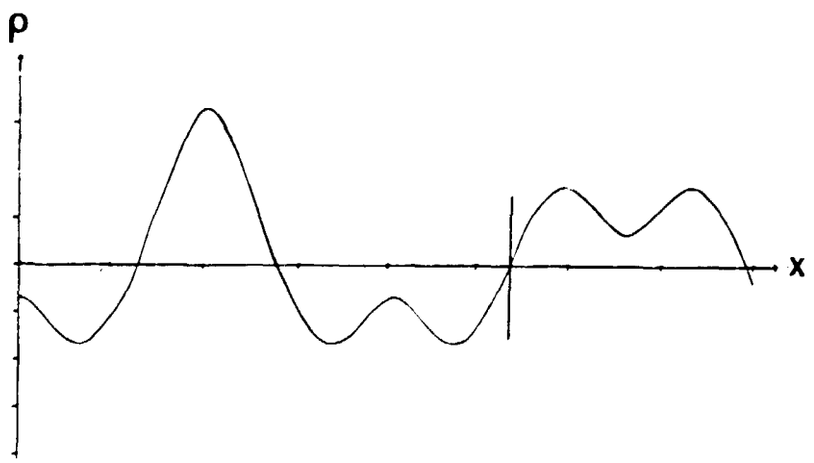

δ=0.016

d

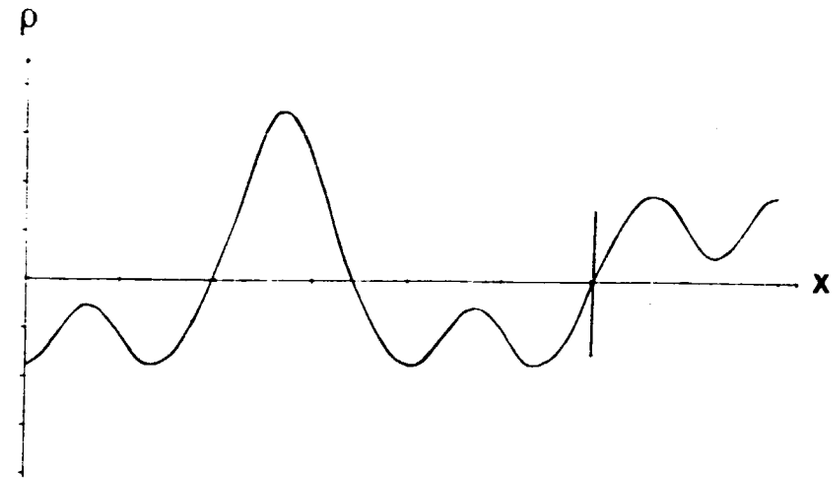

δ= 0.013

e

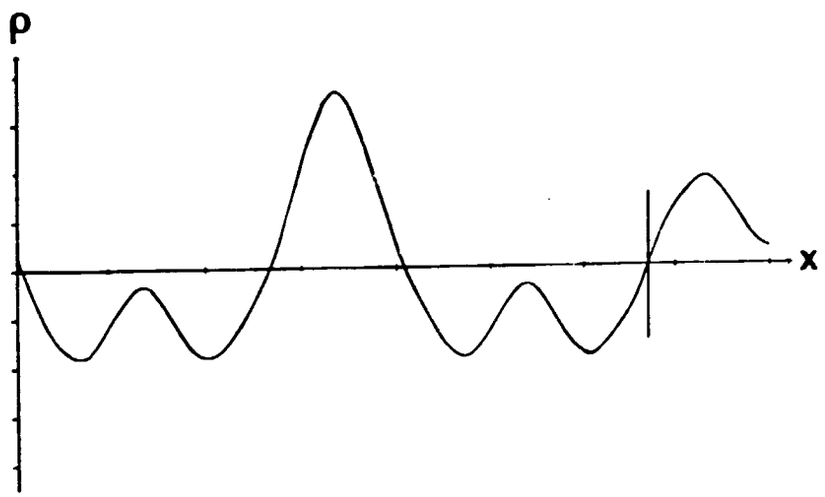

δ= 0.009

f

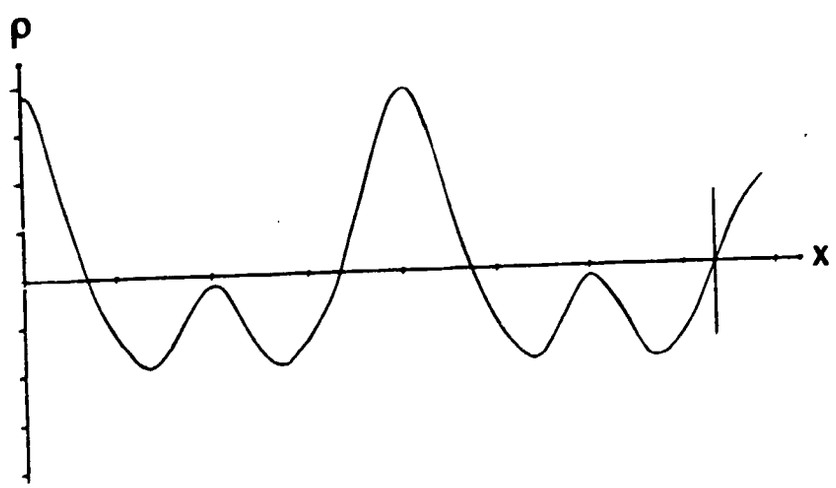

δ= 0.006

FIG 21

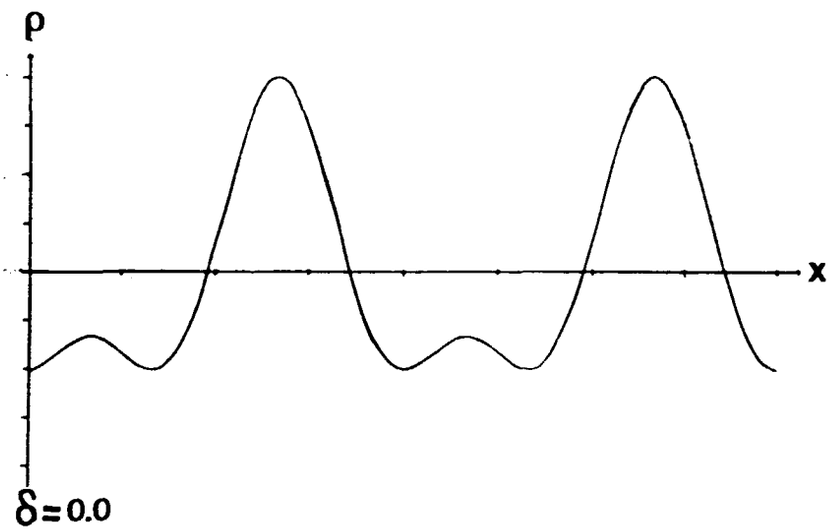

FIG 21

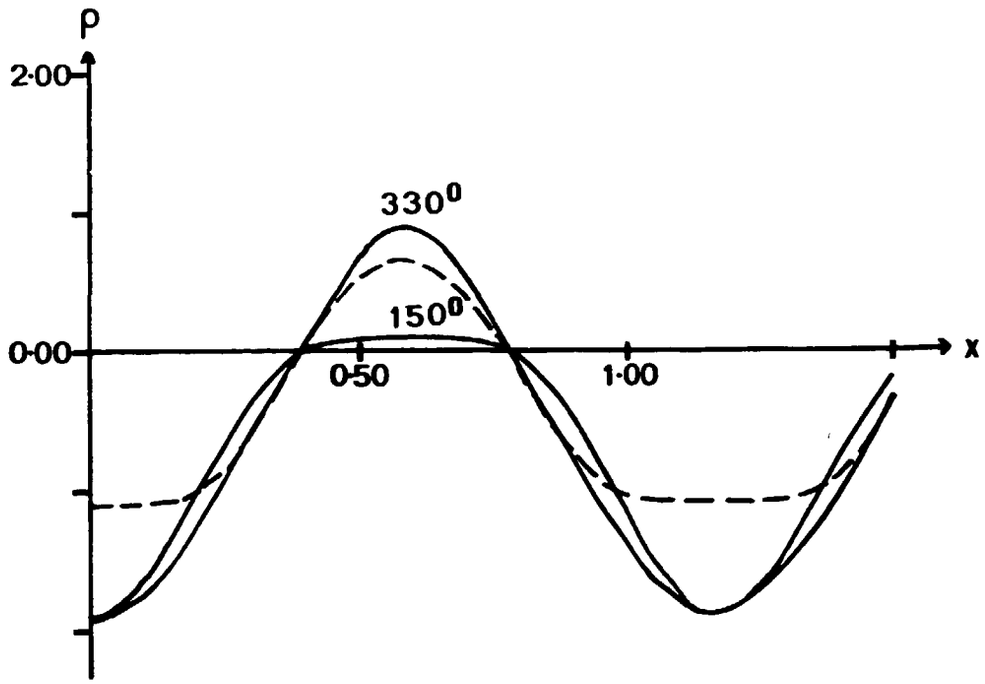

FIG 22

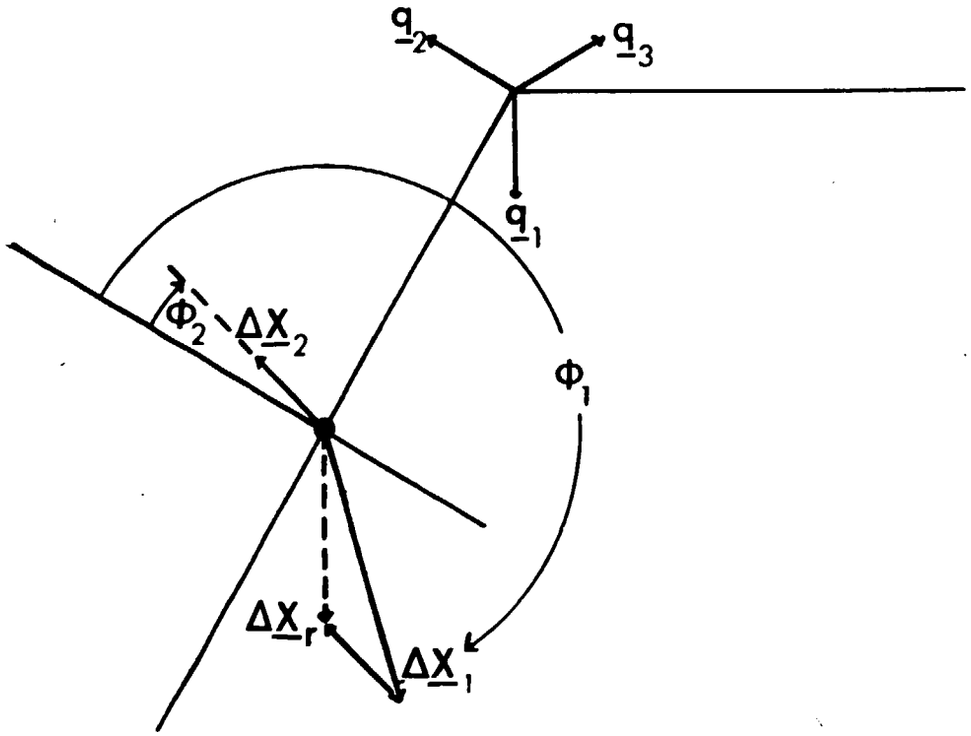

FIG 23

Withers & Burrill, 1980

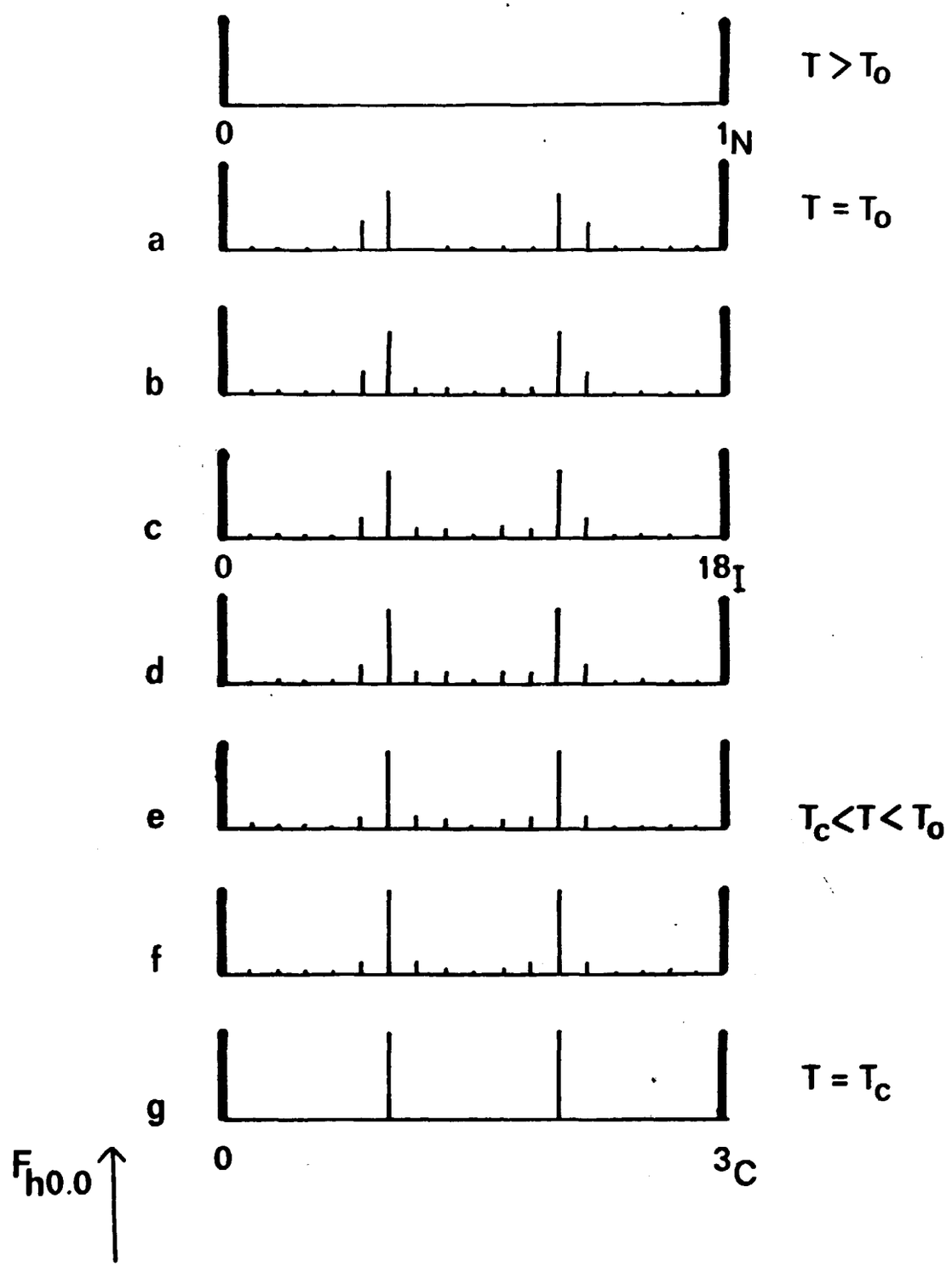

. unobservable

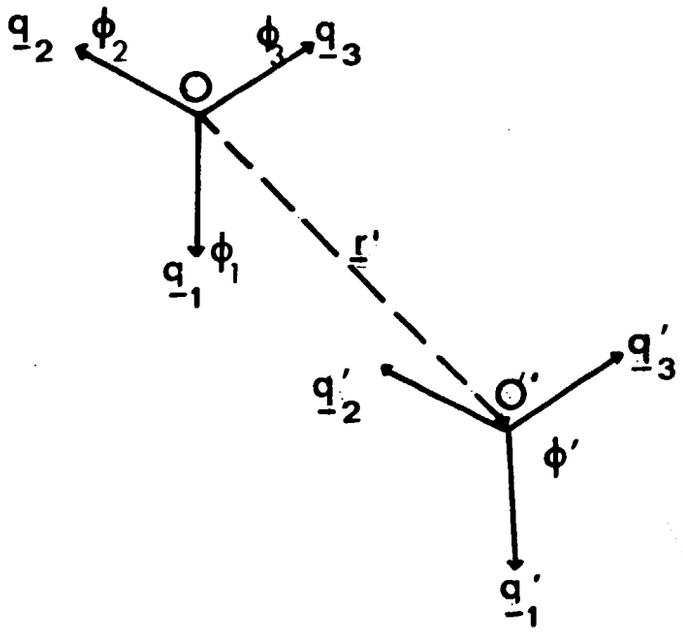
$\underline{q}_2$
ϕ_2
ϕ_3
$\underline{q}_3$
O
$\underline{q}_1$
ϕ_1
$\underline{r}'$
$\underline{q}'_2$
O'
$\underline{q}'_3$
ϕ'
$\underline{q}'_1$

FIG A 1